Journal of Structural Geology 180 (2024) 105085

Contents lists available at ScienceDirect

Journal of Structural Geology

journal homepage: www.elsevier.com/locate/jsg

Structural expression of the frontal thrust of an active fold-and-thrust belt: The Holocene 123-km-long Kur fault, Greater Caucasus, Azerbaijan

Alessandro Tibaldi [a,b], Fabio Luca Bonali [a,b,*], Federico Pasquaré Mariotto [c], Paolo Oppizzi [d], Nino Tsereteli [e], Hans Havenith [f], Gulam Babayev [g], Tomáš Pánek [h]

[a] Department of Earth and Environmental Sciences, University of Milan-Bicocca, 20126, Milan, Italy
[b] CRUST-Interuniversity Center for 3D Seismotectonics with Territorial Applications, 66100, Chieti Scalo, Italy
[c] Department of Human and Innovation Sciences, Insubria University, 21100, Varese, Italy
[d] Meride, 6866, Switzerland
[e] M.Nodia Institute of Geophysics, M. Javakhishvili Tbilisi State University, Georgia, USA
[f] Georisk and Environment, Department of Geology, University of Liège, Liège, 4000, Belgium
[g] Dept. Seismology & Seismic Hazard Assessment, Geology and Geophysics Institute, Baku, Azerbaijan
[h] University of Ostrava, Department of Physical Geography and Geoecology, Chittussiho 10, Ostrava, Czech Republic

A B S T R A C T

Here we present the main features of the frontal structure, known as Kur Fault, of the Plio-Quaternary Kura fold-and-thrust belt in the Greater Caucasus (Azerbaijan). The Kur Fault has been analysed thanks to geological-structural and geomorphological surveys of its whole length, integrated by a relocation of instrumental seismicity, data on historical seismicity, new focal mechanism solutions, and ambient vibration measurements across the fault trace. The in-depth study of the frontal structure can: i) provide insights into the shallow propagation of a regional reverse fault, ii) contribute to a better understanding of the earlier stage of development of a young continent-continent collision, and iii) have implications for seismic hazard assessment because the area is seismically active and hosts the most important infrastructure for energy production in the country. The results show that the fault deforms the surface for a total length of 123 km. The shallow expression is given by four main scarp segments, with a right-stepping arrangement, which have different structural significance; they are represented by an alternation of fault-propagation folds, folds with offset frontal limbs, and shallow faulting. Analyses of the age of deformed deposits and landforms suggest activity from Mid-Late Miocene times to the Holocene. The fault attitude and pure reverse kinematics are coherent with the Holocene and present-day state of stress, characterized by a N–S to NNE-SSW horizontal σ_1, suggesting the capability for seismic reactivation. Calculation of potential Mw indicates values in the range 7.5–7.9 if we consider its entire fault length, 6.1–7.2 if we consider the single segments.

1. Introduction

Contraction at the front of collision mountains can be accommodated by the formation of thrust faults and folds that propagate towards the adjacent basins (Hammerstein et al., 2020). These structures give rise to fold-and-thrust belts that receive a great deal of attention in the literature, as geoscientists attempt to reconstruct the main processes of mountain building. The first models and theories of fold-and-thrust belts have been mostly based on observations of belts that are no longer tectonically active, because inactive areas have been eroded more deeply and thus structures are better exposed, and also for purposes of hydrocarbon exploration. The general geometry and mechanics of fold-and-thrust belts have been investigated in classical works (e.g. Chapple, 1978; Davis et al., 1983) and summarized in review papers (e.g. Butler, 1982; Tavani et al., 2015). Geometry of the frontal part of fold-and-thrust belts has been studied, for example, by field and seismological data (Tibaldi et al., 2023), geophysical surveys (Jones, 1996), geological sections (Vann et al., 1986), numerical (Dean et al., 2013) and analogue models (Bonini, 2001).

Several studies have been devoted also to active fold-and-thrust belts, such as in western Taiwan and in the Himalayan foothills (Hung et al., 1999; Seeber and Armbruster, 1981; Pandey et al., 1995; DeCelles et al., 1998; Thakur et al., 2007), including also the application of tectonic geomorphology to the analysis of landscape evolution and landforms offset (Bull, 2007). Instead, analysis of the frontal structure of active fold-and-thust belts has received less attention and has been studied by different approaches; most studies involved morphometric surveys focusing on the calculation of geomorphic indexes, as first attempted by Bull and McFadden (1977). Other studies involved the analyses of fluid flow at active frontal thrusts (Smeraglia et al., 2020),

* Corresponding author. Department of Earth and Environmental Sciences, University of Milan-Bicocca, 20126, Milan, Italy.
E-mail address: fabio.bonali@unimib.it (F.L. Bonali).

https://doi.org/10.1016/j.jsg.2024.105085
Received 14 December 2023; Received in revised form 1 February 2024; Accepted 12 February 2024
Available online 13 February 2024

palaeoseismological observations (Mugnier et al., 2005; Rajendran et al., 2015), analyses of river terraces (Mukul, 2000; Trexler et al., 2020), analytical approach and drilling data (Suppe and Namson, 1979), and balanced cross sections (Coward et al., 1999). Detailed analyses of emerging/shallow, active thrusts at the forefront of fold-and-thrust systems are more scarce in the literature (e.g. Armijo et al., 2010) and more field data are needed to understand the various possible surface architectures of deposits and structures.

In order to contribute to this topic, we present a detailed description of the Kur Fault, a major thrust located at the front of the Kura fold-and-thrust belt in Azerbaijan (Fig. 1). Here we named the studied structure as Kur Fault in order to follow the local Azerbaijan name and also to differentiate it from the "Kura faults" that are a swarm of strike-slip faults, striking NNW-SSE, located along the Azerbaijan coast of the Caspian Sea, named by Walker et al. (2022). The Kura fold-and-thrust belt constitutes one of the youngest (<3 Ma, Forte et al., 2013; Sukhishvili et al., 2021) tectonic domains in the world and one of the most seismically active areas of the Greater Caucasus, accommodating part of the ongoing convergence between Eurasia and Arabia plates (Forte et al., 2010). The Kura fold-and-thrust belt, in fact, belongs to the foreland main zone of active deformation (Forte et al., 2010; Mosar et al., 2010), as opposed to previous assumption that the main site of shortening is focused along the southern range front of the Greater Caucasus mountains (Philip et al., 1989; Allen et al., 2004). In the last ~1.5 Ma, the Kura fold-and-thrust belt accommodated this convergence at an average rate of 6.7–13.6 mm/yr, based on balanced cross sections (Mosar et al., 2010; Forte et al., 2013; Kangarli et al., 2018). At present, GPS data indicate a shortening across the Kura Basin of ~10 mm/yr (Reilinger et al., 2006; Kadirov et al., 2012; Yetirmishli et al., 2022). In view of the above, our work contributes to a better understanding of the earlier stage of development of a young continent-continent collision, and, moreover, it contributes also to the assessment of seismic hazard in the region. Seismicity based on historical documents in the Kura fold-and-thrust belt, in fact, is widespread and historical events include the 1667 CE earthquake that may have been greater than Ms 6.9 and that completely destroyed the city of Shemakha, killing about 80,000 people (Nikonov, 1982), as well as the destructive earthquakes of 1139 CE, 1828 and 1902 (Ismail-Zadeh et al., 2020; Babayev and Agayeva, 2021).

In spite of the complex geometry and activity of this part of the Greater Caucasus frontal system, neotectonics of the Kura fold-and-thrust belt has received very little attention in the literature. Previous works provided a general description of recent deformation in the area (Mosar et al., 2010; Forte et al., 2010, 2013, 2014; Alania et al., 2017; Sukhishvili et al., 2021) or described very local paleoseismological data of the easternmost part of the belt (Pierce et al., 2022), whereas there is a lack of works in the international literature focusing on the major, frontal WNW-ESE Kur Fault. Sectors of this fault have only been reported in some previous geological maps at a scale of 1:1,000,000 and 1:500,000 (e.g. Bairamov, 2008; Forte et al., 2010). In addition to the above, this fault crosses one of the main Azerbaijan's critical infrastructure: the large Mingachevir and Shamkir hydroelectrical water reservoirs and plant that produce most of the electrical supply to the country (Fig. 2).

Here we give the first detailed description of the Kur Fault in order to characterize its size, geometry, kinematics, age and the possible seismic hazard posed by it. Along its whole length, which we defined to be of 123 km, we carried out structural-geological- and geomorphological surveys during several field missions carried out over the last two years, and integrated these data with a relocation of instrumental seismicity, information on historical seismicity, new focal mechanism solutions, and ambient vibration measurements across the fault trace. Our results allow to define the structure and neotectonic activity of one of the main faults in Azerbaijan, and to contribute to the understanding of the frontal development of an active fold-and-thrust belt.

2. Geological and tectonic background

The collision between the Arabian and Eurasian plates led to an inversion of the relief and the birth of the two orogens of the Greater and Lesser Caucasus, separated by a foreland basin. Timing of the beginning of the collision between Arabia and Eurasia owing to closure of the Neotethys Ocean along the Bitlis-Zagros suture is poorly known, but it is often interpreted as having taken place between the Eocene and

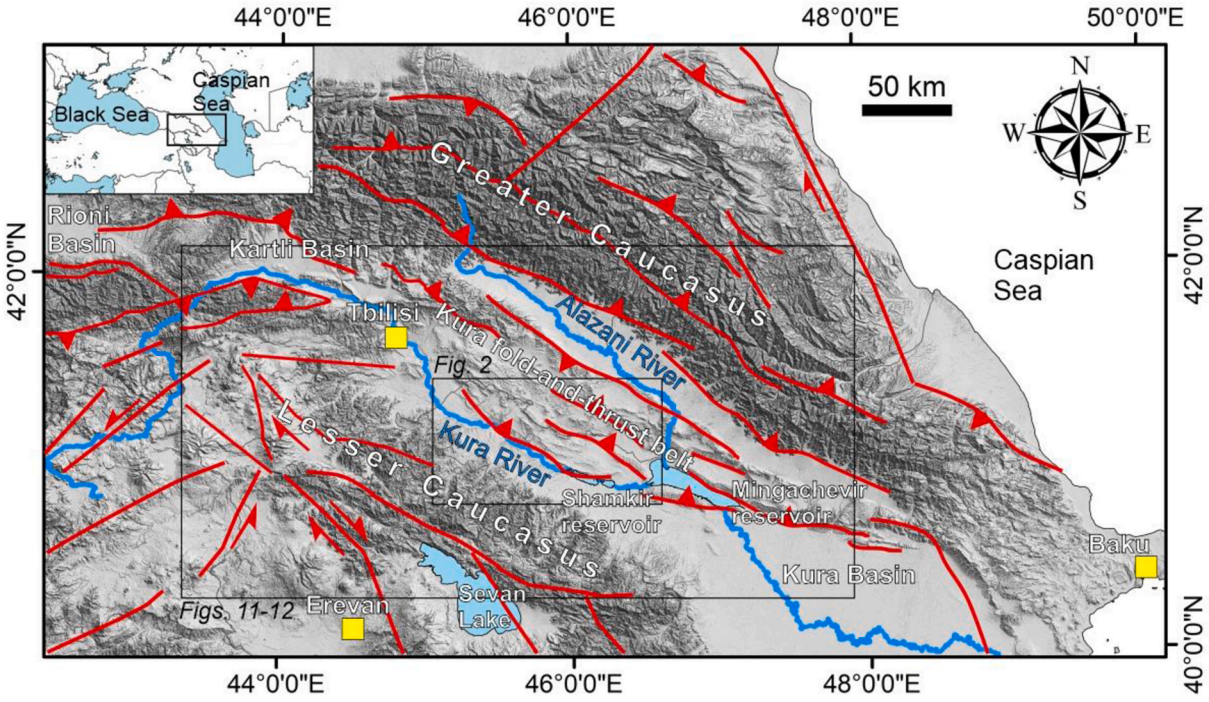

Fig. 1. Location of the Kura fold-and-thrust belt between the two mountain ranges of the Greater and Lesser Caucasus. The two rectangles locate Fig. 2 and 11–12, respectively. Red lines represent main Quaternary faults after Tibaldi et al. (2021). (For interpretation of the references to colour in this figure legend, the reader is referred to the Web version of this article.)

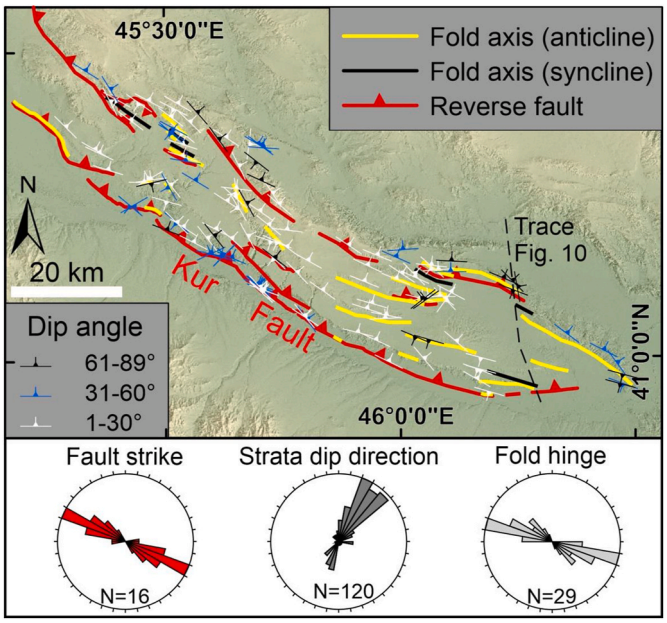

Fig. 2. Structural map showing the bedding attitude of the strata, the main fold axes, and the trace of the major Quaternary faults. The dashed black line provides the location of the trace of the seismic section of Fig. 10. Rose diagrams show azimuthal distribution of reverse fault strike, strata dip, and trend of fold hinge.

Miocene (Agard et al., 2005; Okay et al., 2010; McQuarrie and van Hinsbergen, 2013). The collision of the Arabian and Eurasian plates produced the deformation of about 3×10^6 km^2 of the Earth's crust, and is nowadays one of the largest regions of convergent deformation on Earth (Allen and Armstrong, 2008; Alania et al., 2017). The recent structure of the orogen developed in the Late Cenozoic (in the last 10 million years), but it is still evolving as a result of the northwards movement of the African and Arabian plates at a velocity of 20–30 mm/yr (Reilinger and Barka, 1997). In fact, GPS and seismic data indicate that the convergence between the Eurasian and the African-Arabian plates is still ongoing (Kadirov et al., 2008, 2012; Avagyan et al., 2010; Adamia et al., 2017; Sokhadze et al., 2018). As a result, the Greater Caucasus and the Lesser Caucasus are still tectonically active, with vertical and horizontal components of displacement that result in present-day, active orogenic processes (Koçyiğit et al., 2001; Allen et al., 2004; Reilinger et al., 2006; Tan and Taymaz, 2006; Pasquaré Mariotto et al., 2011; Kadirov et al., 2015; Tibaldi et al., 2017a, 2017b, 2020).

Paleogene, Neogene and Quaternary strata in sedimentary basins along the southern flank of the Greater Caucasus typically consist of clastic marine to terrestrial sedimentary rocks, reflecting a generally shallowing depositional setting through time (Trexler et al., 2022). These basins include the Rioni and Kartli basins in the western and central Greater Caucasus, and the foreland Kura basin in the east (Banks et al., 1997; Forte et al., 2013) (Fig. 1). South-directed fold-and-thrust belts within these flanking basins expose Cretaceous-to Neogene-age strata. Surface geology and seismic-reflection data suggest that the fold-and-thrust belts have a thin-skinned structural geometry (Banks et al., 1997; Forte et al., 2010; Alania et al., 2017, 2022; Adamia et al., 2017; Tibaldi et al., 2017a; Tari et al., 2018; Trexler et al., 2023) and are presently active (e.g., Banks et al., 1997; Forte et al., 2013; Tibaldi et al., 2018; Trexler et al., 2020). Prior work on the structural architecture of the Greater Caucasus assumed that the main site of Cenozoic shortening was located along a dominant, deeply rooted structural system referred to as the Main Caucasian Thrust (MCT), which was placed by different authors either at the base of the crystalline basement in the core of the range, or in the marine sedimentary package of the Caucasus Basin to the south, or at the southern topographic range front (Saintot et al., 2006; Mosar et al., 2010; Adamia et al., 2011). Neotectonic investigations of active fold-and-thrust belts in the eastern (Forte et al., 2010, 2013; Kadirov et al., 2012) and western (Banks et al., 1997; Alania et al., 2017; Tsereteli et al., 2016; Tibaldi et al., 2017b) Greater Caucasus suggest that the MCT (e.g., Vasey et al., 2020) may indeed be regarded as a significant lithotectonic boundary within the Caucasus orogen, but it is unlikely to be the site of main active defomation or dominant orogenic structure at the surface. The fact of the matter is that geological and structural observations in the region indicate that faults within the orogen are steeply dipping; therefore, they are not favorably oriented to accommodate present-day observed tectonic shortening. In fact, these faults also appear to have produced little horizontal displacement, and this puts in doubt whether they play a major role in the modern mountain range (Trexler et al., 2022). Besides, geologic, geodetic, and seismic observations suggest that major present-day convergence within the Caucasus system occurs primarily across the intervening basins (Jackson, 1992; Berberian, 1997; Reilinger et al., 2006; Forte et al., 2010, 2013, 2014; Karakhanian et al., 2013). In particular, it has been postulated that, since the Plio-Pleistocene (Forte et al., 2010), convergence along the eastern Greater Caucasus (i.e., ~46–48°E) has been accommodated mainly along the Kura fold-and-thrust belt, a series of sub-parallel, north-dipping, low-angle thrusts that are present well south of the main southern slope of the mountain chain (Forte et al., 2010, 2013, 2015). It needs to be pointed out that, prior to the initiation of the Kura fold-and-thrust belt, deformation was accommodated along an emergent thrust, or series of thrusts, near the present Greater Caucasus range front (Forte et al., 2013). So, while there is evidence that the Greater Caucasus accommodated >200 km of shortening in the early Cenozoic, the Kura fold-and-thrust belt has accommodated 30–40% of Arabia-Eurasia convergence since the Pliocene and it is presently the main place of shortening within this area (Forte et al., 2010). The eastern portion of the Kura fold-and-thrust belt is marked primarily by south-vergent folds and thrusts that involve up to Pliocene-to Quaternary-aged sediments. The geometry of these structures is compatible to shear folds that form above propagating thrusts and root to a shallow detachment (Forte et al., 2013).

Our study focuses on the eastern (~45°E–48°E) part of the Kura fold-and-thrust belt, mostly located in Azerbaijan (Fig. 1). The elevation of the area reaches about 1000 m in the western part and decreases towards the east, where the ridges have an altitude of approximately 200 m. Most of the area consists of hilly land, with valleys reaching a maximum depth of approximately 100 m. The area is bordered to the south by the Kura River valley and to the north by the Alazani River basin. Here, Quaternary sediments of the Kura River basin form a westward embayment of the Caspian basin system (Nalivkin, 1976b; Forte et al., 2015). The western and higher part of the studied area is more intensely exhumed, and Miocene sediments from the Sarmatian, Maeotian and Pontian stages mostly crop out. The eastern part of the area is characterized by sediments from the upper Pliocene Akchagyl and lower Pleistocene Apsheron regional stages with thickness of several hundred meters (Forte et al., 2015). These sediments are made of clast-supported conglomerates at the base of the Akchagyl, then alternances of massive sandstones, silty claystones, clavey siltstones and volcanic ash (Forte et al., 2015). Furthermore, in the same region that we studied, Alizadeh et al. (2016) discovered complete and faunistically rich sections. In these sections, Upper Pliocene deposits are represented by layers of sandstones and claystones with bivalves and volcanic ash. The thickness varies from 113 m to 205 m. The same authors describe the Lower Pleistocene made of claystones, sandstones, conglomerates, and volcanic ash. They belong to the Apsheron regional stage with a lower boundary fixed at 1.7 Ma. Lazarev et al. (2019) illustrate the uppermost layers of the Middle Pleistocene near our study area, by describing the Goychay section (already logged and described in detail by Forte et al., 2013); this succession is made of conglomeratic beds interbedded with dark grey and reddish brown claystones. Dark grey

claystones include centimetre-scale vertical roots and contain some centimetre-thick coal layers, and terrestrial gastropods. The sandstones were deposited under very high energy in fluvial channels. In between these fluvial channels, organic-rich fine-grained sediments were deposited out of suspension in flood plains. Therefore, this succession was deposited in fluvial and floodplain environments. In the Kura depression, Upper Pleistocene deposits (Khvalinian horizon) developed in both marine and continental facies. Marine deposits occupy the eastern sector of the depression and are expressed by claystones, siltstones and sandstones (50–60 m). To the flanks of the depression, they are replaced by river deposits (detrital cones and terrace remains). Generally, the sequence is topped by very loose conglomerates that rest in discordance, or by eluvium-colluvium deposits. Most of the sediments in the studied area, of Pliocene and Quaternary age, can be characterized as weak and poorly lithified (Pánek et al., 2024).

3. Methods

3.1. Field survey and data collection

The structures of the study area were firstly defined with the aid of photointerpretation of GoogleEarth images, as well as by the analysis of 30-m Digital Surface Model (http://www.eorc.jaxa.jp/ALOS/en/aw3d30/; Takaku et al., 2020). The results have been integrated with field surveys at the mesoscale, where major structures (lengths in the order of kms) were measured and mapped, and at the local scale, where faults with cm offsets and veins with crystal fibers growth were studied. We also measured systematically the dip of the strata dividing them between the older marine deposits and the younger continental deposits, with reference to published ages. Based on reversals in bedding dip direction and the alignment of points of maximum curvature along marker beds, we identified the trace of anticline and syncline axes. By doing so, we reconstructed the geometry of the main folds and evaluated the more recent deformations. This survey has been necessary for understanding the general architecture of this belt in relation to its frontal fault, which is represented by the Kur Fault. All data have been recorded in a GIS environment.

Faults were measured in the field wherever possible. Special attention was dedicated to the Kur Fault that was surveyed in the field systematically, as we tried to reach the fault zone as much as possible along its whole length of 123 km. Classical morphotectonic observations related to recent/active faulting were carried out, including the search for triangular facets, escarpments, hanging river gullyes, truncated strata, tilted/folded young deposits and landforms, etc. (Burbank and Anderson, 2001; Keller and Pinter, 2002; McCalpin and Carver, 2009). At one site, we found a natural exposure in a trench excavated by a creek, crossing perpendicularly the Kur escarpment; in this trench it was possible to observe and measure the Kur Fault plane reaching the surface.

In regard to local scale observations, we carried out measurements of the geometry and kinematics of secondary faults, of tectoglyphes on fault planes to assess the net slip, and of crystal fibers growth in veins. For secondary faults and veins we focused on distinguishing post-folding and post-main faulting structures, based on their crosscutting relationships, which should correspond to the youngest deformations.

3.2. Earthquake epicenters, magnitudes and focal mechanism solutions

We updated and combined different local catalogues from several sources to compile a complete catalogue of earthquakes with Mw equal or greater than 3. The catalogue covers the period from 1250 BS until 2022 for Georgia and until 2020 for Azerbaijan. From 1250 BS to 2006, the main source of the compilation of the earthquake catalogue is the earthquake databases of the Institute of Geophysics at I. Javakishvili Tbilisi State University (IGTSU) of Georgia. IGTSU was the centre of seismic data processing in the Caucasus until 1979, and produced a catalogue named TIF. From 1980 all republics of the Caucasus processed seismic data and independently published catalogues for their own territories. From 1980 till 2005 the main sources of seismic data in Georgia was the Seismic Monitoring Centre of the Institute of Geophysics, Georgia (SMCIG). Until 2010, the National Seismic Monitoring Centre of ILIAUNI provided the complete earthquake catalogue for Georgia. After 2010, initial national waveform data as well as information on small earthquakes with Ml < 3 are not freely accessible. For this reason, the International Seismological Centre (ISC), the European-Mediterranean Seismological Centre (EMSC), and National Agencies of neighboring countries have been used for updating catalogue after 2010.

In regard to the homogenization of the earthquake magnitude scale in the entire Caucasus region, energetic parameters of earthquakes were estimated in terms of surface waves (indicated in the catalogue as M_{LH} or Ms) mostly for moderate to strong earthquakes with Ms ≥ 4.0 using the regional calibration curve for Ms and from 1961 to 2003 in terms of energy class (K) for small and moderate earthquakes and, whenever the direct determination of Ms was impossible, the size of events was estimated according to the equation Ms $=$ 0.56 K–2.2, based on Rautian (1964). Following Rautian and Khalturin (1978), it is accepted that Ms $\cong$ Mc, where Mc is the magnitude estimated from coda waves. Sometimes, Mb (body wave magnitude) $\cong$ Mpv (magnitude estimated from the vertical component of p waves) was also assumed. There is an empirical correlation formula between Mpv and Ms for the hereby considered region: Mpv $= 2.5 + 0.63$Ms. So, until 2003, the earthquake catalogue for the Caucasus was unified to Ms. Homogenization of the earthquake catalogues in terms of moment magnitude (Mw) was accomplished by using new conversion equations that were developed on national data by Onur et al. (2019), Tsereteli et al. (2021), Tibaldi et al. (2020) and by ourselves. We used regional conversion equations or equations from neighboring countries with similar tectonic settings for those magnitudes for which no conversion equations were derived based on national data. On the ISC data, a new conversion eq was developed between Ml (locale magnitude) and Mpva (regional magnitude of body waves determined by the P-wave recorded by short period instruments) that enables evaluating the relationship between Mw and Mpva using conversion eq between Mw/Ml.

As regards the determination of the new focal mechanism solutions (FMS), the first motion polarity technique was used. Only earthquakes for which the number of polarities is equal or greater than 8 and azimuthal gaps are $<180^{\circ}$ were included in the analysis. Data have been collected from the bulletins of the Institute of Geophysics of Tbilisi (Georgia). First, the hypocentral parameters of the earthquakes were calculated using the HYPO - 71 program (Lee and Larh, 1975), as the accuracy of fault plane solutions depends on precise hypocenter determination. For the calculation from first motion polarities, which is based on a maximum likelihood algorithm, we used the software package FA2002 by Lander (2004). For more details on the methodology, see Tsereteli et al. (2016). P-axes from these new FMS were also plotted together with other already published FMS and with σ_1 directions from the World Stress Map (www.world-stress-map.org/).

3.3. Ambient vibrations measurements

The ambient noise wave field is formed by the combination of surface waves through the interference of P- and S-waves in the upper layers (Lachet and Bard, 1994; Bard et al., 1999). As the ambient noise is associated with surface waves, the method alone can provide quantitative values of the fundamental frequency but only qualitative estimates of the amplification potential associated with the observed resonance peaks (Havenith et al., 2002). Ambient noise measurements can be completed by a group of sensors or by a single station so-called 'H/V' measurements. Here, we focus on the latter that have become a powerful geophysical exploration method in recent years. First introduced by Nogoshi and Igarashi (1970) and further developed by Nakamura

(1989), Lachet and Bard (1994) and Bard et al. (1999), the method uses the spectral ratio of the horizontal and vertical components of seismic background noise from natural and anthropogenic sources to determine the resonant frequency f0 with the help of a seismometer (Nakamura, 1989). The calculation of the H/V ratio based on the Fourier spectrum of the ambient noise vibrations is completed according to the following steps: i) the ambient noise is recorded by a seismometer in the following three components, the two horizontal (north-south, N, and east-west, E, direction) and the vertical (Z) one. ii) Then, time windows of 8–30 s are defined along the recorded signals and those presenting transient and spurious noise (typically related to local artificial sources) are excluded from the analysis. For each remaining window, a Fourier amplitude spectrum is calculated and smoothed. iii) Finally, the ratio between the averaged spectra of the horizontal components H(f) and the one of the vertical component Z(f) is computed for each window. An average ratio can then be calculated, combining the inputs from all time windows. For sites marked by stronger seismic contrasts in the underground, one clear peak at the fundamental frequency, f0, with an amplitude peak, A0, can be identified from this averaged spectral ratio (Bonnefoy-Claudet, 2004). In a simple geological context composed of one horizontal soft soil layer overlying bedrock, the resonance frequency, f0 (Hz), is associated with the thickness of the surface layer, h (m), according to the expression:

$$f0 = Vs/(4*h) \quad (1)$$

Where Vs is the velocity of the S-wave (in m/s) of the upper soft layer.

If Vs can be assessed from other geophysical methods (or, as here, Vs is estimated from the type of outcropping deposits), this H/V analysis can help determine the thickness h of the layer on the basis of Equation (1): h = Vs/(4*f0). Thus, the purpose of this method is to identify the thickness of the upper soil layers. In the case of this study, we define some changes of the thickness of the deposits on either side of the fault as already shown by Demanet et al. (2001) in another region.

In total 15 H/V measurements were completed across the Kur fault scarp with two TROMINO 3G seismographs (working in parallel) to record the ambient seismic noise over the different sites. We used the three velocimetric channels of the TROMINO 3G stations for this analysis in addition to the built-in GPS receiver. During installation, small holes were drilled to guarantee adequate coupling of the sensors with the soil. Measurements of 20 min were made at each site; detailed information (name of site, location, duration of measurement) is presented in Table 1, while the trace of the sites of measurement is reported as 13 in Fig. 3.

The data of the 15 H/V measurements were processed by the GEOPSY program (Wathelet, 2005; Wathelet et al., 2020). While processing, we noted that a series of computed H/V spectral ratios presented multiple peaks that can be related to different subsurface seismic velocity contrasts: for instance, shallower interfaces produce higher peak frequencies, while thicker layers produce lower-frequency resonance peaks. Detecting the relations between interfaces and peak frequencies was among the goals of this study.

Table 1
Coordinates of the point measurements at the active faults.

station name	Longitude	Latitude	Elevation	Duration
AZ_AF_ST1	45.700555	41.111111	170	20
AZ_AF_ST2	45.701135	41.111864	168	20
AZ_AF_ST3	45.701944	41.112512	180	20
AZ_AF_ST4	45.702505	41.112936	174	20
AZ_AF_ST5	45.703055	41.113333	180	20
AZ_AF_ST6	45.703608	41.113614	187	20
AZ_AF_ST7	45.704166	41.113888	200	20
AZ_AF_ST8	45.704994	41.114083	207	20
AZ_AF_ST9	45.705277	41.114444	210	20
AZ_AF_ST10	45.705716	41.114745	207	20
AZ_AF_ST11	45.706388	41.115277	200	20
AZ_AF_S12	45.707767	41.116084	192	20
AZ_AF_ST13	45.707222	41.115555	190	20
AZ_AF_ST14	45.709879	41.117494	176	20
AZ_AF_ST15	45.708888	41.116666	190	20

4. Results

4.1. Regional structural geological data

The results are reported in Fig. 2 in the form of a structural map showing some of the measured bed attitude of the strata (the most representative for each area), the trace of the major faults and the main fold axes. The main faults run parallel to the mountain range and to the folds. In the studied area, it can also be observed a slight anticlockwise rotation of fault strike from west to east: in the western part, faults strike mostly in the range N125-170°E, in the central part in the range N123-145°E, and in the eastern part in the range N90-117°E. The few observed main reverse fault planes are quite steep, in the order of 70–79°, and are in the interior of the fold-and-thrust belt, suggesting that they may be originally shallower-dipping reverse faults that were tilted later on. Some strike-slip faults were also observed, but they are short and have small offsets, in the order of cm-dm, and thus can be considered very local secondary structures; they will be described in the section on local structures. The length of the main reverse faults ranges from 6 to 39 km, apart from the Kur Fault; as will be discussed later, the Kur Fault can be considered longer as a unique structure, although at the surface it is divided into four segments. Out of the 16 recognized main faults, 15 dip to the NNE and show reverse motions, consistent with the vergence of the folds. Only one main fault, about 10 km long, dips towards SSW (located in the northwesternmost portion of the studied area) and thus can be considered a backthrust. Another main backthrust has been recognized in the field but its outcrop trace is too short to be drawn in Fig. 2. In some cases, in correspondence of NNE-dipping reverse faults, the hanging wall block is marked by strata dipping to the NNE or NE, thus parallel or subparallel to the fault plane.

We recognized 29 main folds at the regional scale, with length from 2 to 21 km. The fold axes trend dominantly from WNW-ESE to NW-SE. The fold interlimb angles are from open to close, and most folds show a vergence towards SSW, as indicated by southern limbs that have a steeper geometry than northern limbs, consistent with previous authors (Dotduyev, 1986; Philip et al., 1989; Tevelev and Blyumkin, 1990; Forte et al., 2010), wheras the other folds are symmetrical. In some places, the southern fold limb has a vertical attitude. Anticlines dominate over synclines. The areas between the main folds are characterized by a monoclinal geometry with strata essentially dipping in the range NNE to NE. In the uppermost part of the succession, late Pleistocene-Holocene continental deposits are widespread and show a bed dip in the order of 1–9° towards NE. Some folds are located immediately north of major reverse faults, i.e. some faults are located along the anticline southern limbs, suggesting a direct relationship, whereas other folds are not close to outcropping faults. Due to the age of the rocks involved in folding, the fold age can be attributed mainly to the Plio-Quaternary, although previous deformation cannot be ruled out, as will be described later. Minor folds, which for scale reasons were not possible to map in Fig. 2, have also been found. They have hinge lines parallel to the main folds and again show a vergence to the south.

4.2. Kur fault

4.2.1. Morphotectonic and structural data

All the sites that can be reached along the trace of the Kur Fault have been studied. The remaining portions have been analysed through GoogleEarth images and DSM. Field observations allowed us to recognize a series of clues that suggest the presence of an active reverse fault, dipping to the NNE. In order to avoid repetitions, only the most representative sites will be described hereunder, giving the evidences and the geometry of the deposits of the hanging wall block. The location of the

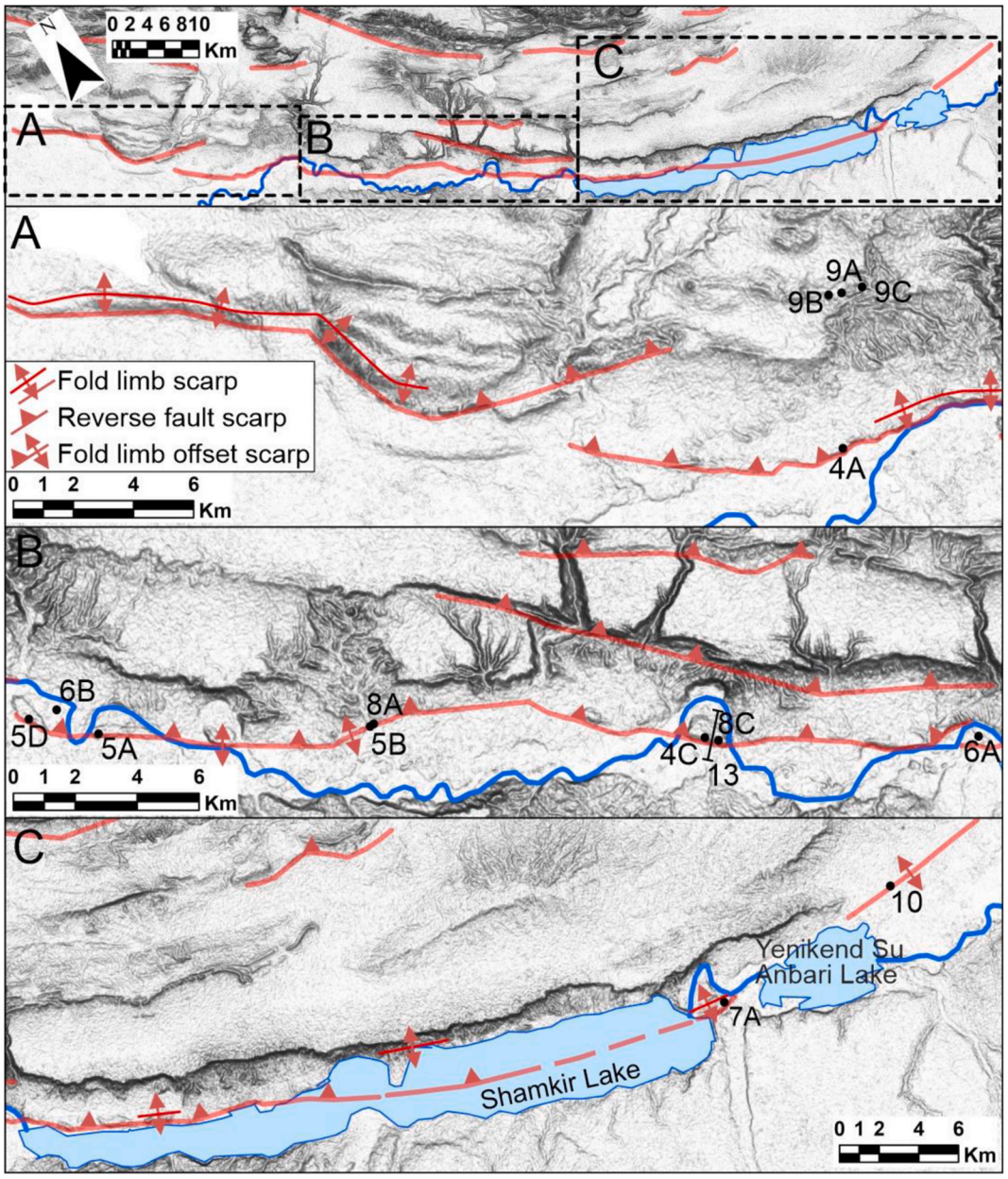

Fig. 3. Detailed structural map of the Kur Fault, classified based on the significance of the escarpment as a function of the geometry of deposits of hanging wall blocks and emersion of the fault plane. Black dots and numbers indicate the localities of the corresponding figures. DEM from NASADEM at https://lpdaac.usgs.gov/products/nasadem_hgtv001/, resolution 30 m.

described sites/figures is shown in Fig. 3.

At the site of Fig. 4A and B, there is an outcrop located along the trace of the Kur Fault. Here, on the hanging wall block of the possible fault plane, there are alternating siltstones, sandstones and conglomerates that can be attributed to the Pleistocene. The strata dip 38° southward. Above the Kur scarp, the topography creates a gentle upward curved surface elongated parallel to the fault strike. A few hundreds meters to the ESE along the Kur Fault, the topography shows a clearer curved surface. An outcrop here shows that this curved topographic surface coincides with the attitude of loose conglomerate deposits that create an anticline. The southern limb is characterized by strata dipping N150° with an inclination of 20°; the northern limb dips N353° with inclination of 19°.

The location of Fig. 4C and D shows another outcrop located along the Kur Fault more to the ESE. This example is characteristics of another geometry of the deposits, different from the previous example. In this case, the deposits dip northward like the fault, and the fault scarp is located immediately south (on the left of the picture). The lower part of the exposed succession is made of siltstones and sandstones of Pliocene?-Pleistocene age, tilted about 27°. Above there are loose conglomerates in discordance that can be attributed to the Upper Pleistocene-Holocene. The bedding surface of the conglomerates is also tilted northward attaining an inclination of 6°.

At the site of Fig. 5A, we can observe one of the zones where the Kur Fault crosses the Kura River. Here there is a clear morphological high delimited to the south by a 7 m high scarp. This scarp is perfectly aligned with other similar evidences to the east and west, thus it coincides with the trace of the Kur Fault. A series of uplifted river terraces is located north of the Kur escarpment and represents a morphological high, i.e. they are located on the fault's hanging wall block. Uplifted river terraces can also be recongized in the forefront of the photo of Fig. 5A and can be in part correlated with the terraces shown in the background. The

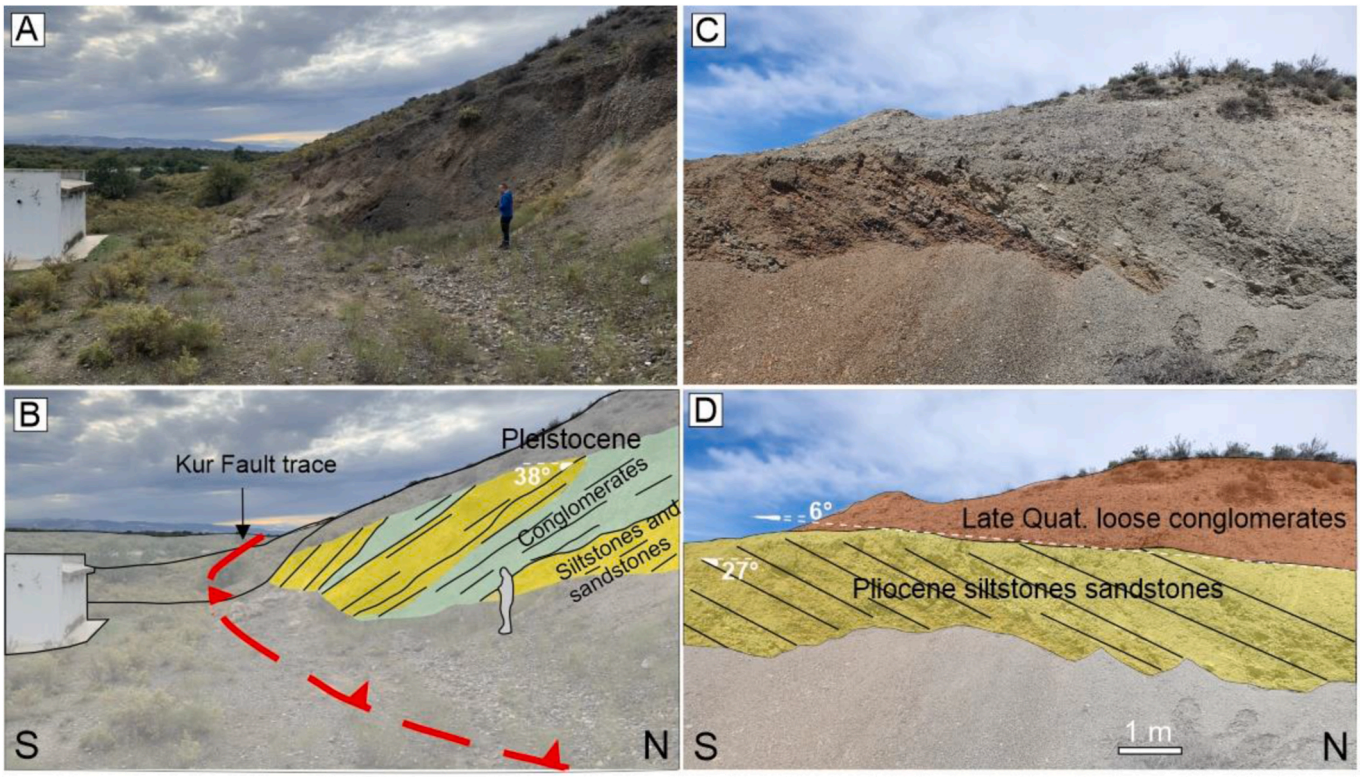

Fig. 4. (A) Photo and (B) interpretation of an outcrop located along the trace of the Kur Fault. Here an alternance of Middle-Upper Pleistocene siltstones, sandstones and conglomerates is tilted southward. Man for scale. (C) Photo and (D) interpretation of another outcrop located along the Kur Fault. In this case the deposits dip northward like the fault. They are made of siltstones and sandstones of Pliocene?-Pleistocene age, above which there are loose conglomerates in discordance. Location in Fig. 3.

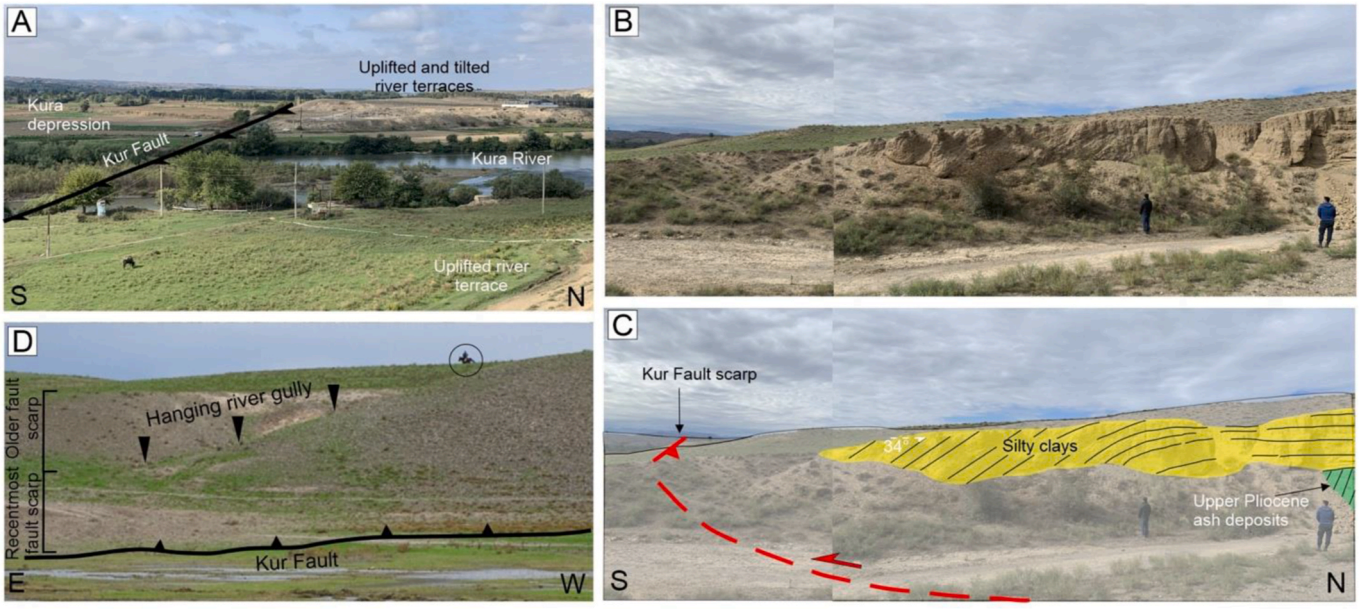

Fig. 5. (A) Uplifted and tilted late Quaternary river deposits along the Kur Fault. (B) Photo and (C) interpretation of folded silty clays, resting in discordance above Upper Pliocene deposits, along the Kur Fault trace. (D) Presence of hanging river gullies (black triangles) along the Kur Fault scarp, an evidence of very recent tectonic activity. Circle indicates a horse, in background, for scale. Location in Fig. 3.

deposits underlying these terraces are made of loose fluvial conglomerates. The fluvial beds are not horizontal but they dip of a few degrees to the NNE. Also the present topographic surface at the top of the morphological high dips 4° to the NNE. These fluvial terraces are not present south of the Kur Fault trace. The Kura River creates a meander sourrounding the morphological high. The river enters the meander along a gap in the trace of the Kur Fault that here shows a right-stepping geometry. This relationship between a fluvial meander and the stepping arrangement of the Kur Fault has been observed in other cases along the structure and has been highlighted in Fig. 6. Regarding the age of these

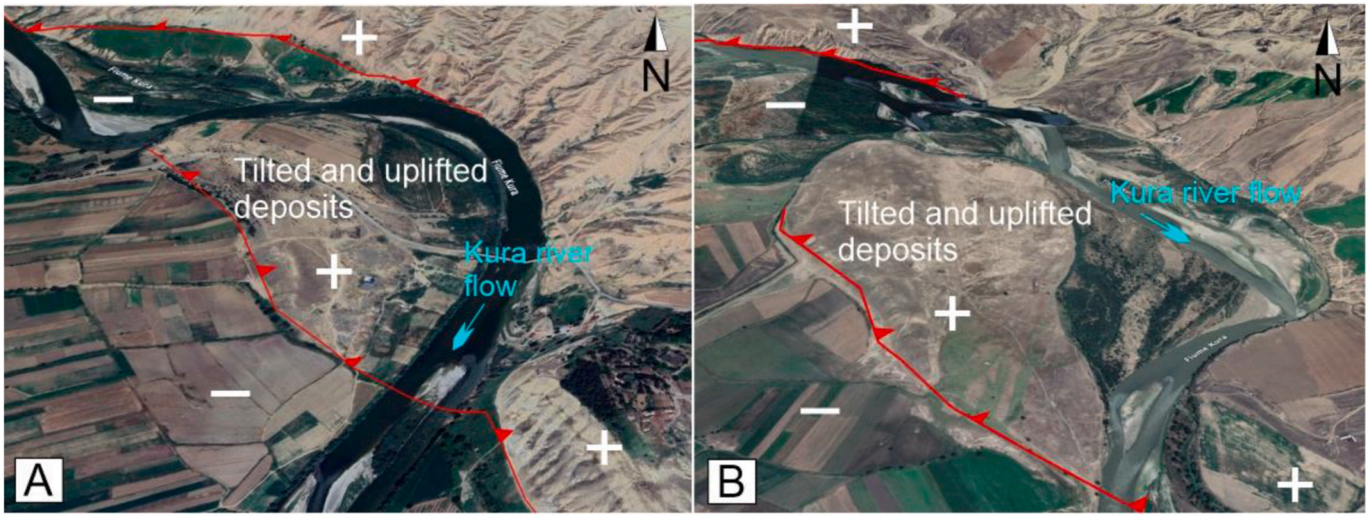

Fig. 6. GoogleEarth images of meanders of Kura River. In both examples, the river flows into the zone left by the right-stepping arrangement of the Kur Fault (in red). Symbol + indicates uplifted zone, - indicates relatively lower zone. Location of A and B in Fig. 3. (For interpretation of the references to colour in this figure legend, the reader is referred to the Web version of this article.)

terraces, we have to point out that the Kura river deposits were dated in an area immediately west of the Kur Fault by von Suchodoletz et al. (2016). Radiocarbon and luminescence dating gave ages between 41.5 and 11.2 cal Ka BP, but more recent terraces can also be present.

At the site of Fig. 5B,C, a 5-m-high scarp delimits to the north a topographic high where a succession of sedimentary deposits is folded. The lower part of the exposed succession is rich in ash fall deposits that are characteristic of the upper Pliocene (Alizadeh et al., 2016). These deposits dip 70° to the SW. The ash deposits are truncated by an angular unconformity above which there is a succession of poorly consolidated silty clay deposits that can thus be ascribed to the Quaternary. These deposits are horizontal in the northern part of the section and become steeper approaching the Kur Fault scarp. Near the scarp, these recent-most deposits attain a dip of 34° to the SW.

The site of Fig. 5D is also representative of various other localities along the Kur Fault that have the same characteristics. The escarpment of the Kur Fault can show a differentiated morphostructural aspect in the upper part if compared to the lower one: above, the scarp is incised by small dry river gullies creating triangular facets, whereas the lower part is more continuous and with rarer gullies. In some places, as the site of Fig. 4D, the river gullies are hanging above the more continuous scarp. In this site, the upper scarp is about 13 m high, and the lower scarp is 1 m high.

At the site of Fig. 7A and B, deposits of different age show different degrees of tilting, depicting an anticline structure with a hinge line trending WNW-ESE. This fold is located immediately north of the possible trace of the Kur Fault. In the western part of the anticline, strata of Pliocene-Pleistocene (?) age crop out and dip steeply to the south. Here we can only infer that they represent the southern limb of the Pliocene-Pleistocene (?) anticline because the northern limb is covered by younger strata. The upper succession is composed of fluvial conglomerates of dark grey colour whose dip attitude coincides with the topography. Such conglomerates rest in discordance over the Pliocene-Pleistocene (?) deposits. In the southern part of the structure, the conglomerates dip 16° to the south (Fig. 7B), whereas further north they dip, with a similar attitude, in the opposite direction constituting the northern limb of the anticline. These conglomerates are very poorly cemented and represent the uppermost deposits in most of the Kura fold-and-thrust belt, and are locally covered only by eluvial-colluvial deposits. Based on their characteristics, stratigraphic position, and

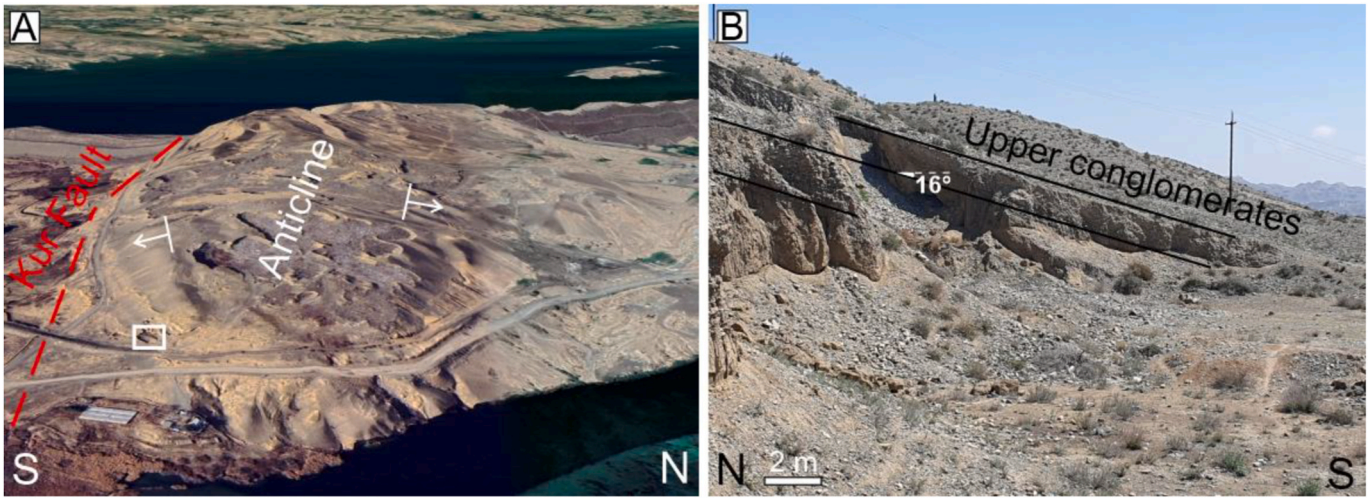

Fig. 7. (A) Anticline located along the surface projection of the Kur Fault (red line), near the Shamkir dam. Location in Fig. 3 (B) The tilted conglomerates of fluvial origin along the Kur Fault compose the southern limb of the anticline (location in the small box, left hand image). (For interpretation of the references to colour in this figure legend, the reader is referred to the Web version of this article.)

geometric relationships with the underlying deposits, we can infer that these conglomerates have a late Pleistocene-Holocene age.

4.2.2. Slip planes along the Kur fault

At the site of Fig. 8A and B, strata of Early Pleistocene age are tilted 29° to the north and crop out immediately north of the Kur Fault scarp. Here, the strata are also offset by two converging reverse faults that create a pop-up structure. The northern fault dips 20° to the south, and splays from the other fault that dips 68° to the north. The more continuous north-dipping fault offsets by 40 cm also the base of eluvial very recent (late Holocene?) deposits, as can be seen in the detail of Fig. 8B. These deposits rest in discordance above Early Pleistocene deposits and mantle the present-day topography.

We found an open trench across the Kur Fault at the site of Fig. 8C, which allowed us to carry out direct observations of this structure. This trench, which is of natural origin due to localized erosion, is about 3 m large and 10 m long. In proximity of the northern termination of the trench, it has been possible to observe directly the emersion of the slip plane of the Kur Fault. The fault plane dips N30° with a dip angle of 35°. Although the fault plane arrives very close to the topographic surface, it does not affect the present soil. Along the fault plane, it has been possible to find tectogliphes; striations and other kinematics indicators are compatible with pure reverse motions with a pitch of 90°.

4.2.3. Local scale observations

In some outcrops the presence of minor faults has been observed, with offsets in the order of cm. Here we report a couple of examples. The site of Fig. 9A corresponds to a horizontal outcrop resulting from excavation in an open mine. The rocks are composed of sedimentary strata whose characteristics allow to ascribe them to the Late Pliocene. Here there are two sets of strike-slip faults: one set is composed of NNW-SSE-striking vertical planes with right-lateral strike-slip offsets in the order of 1–10 cm. The other set strikes NNE-SSW with vertical planes and left-lateral strike-slip offsets of similar magnitude. They show mutual crosscutting relationships indicating they are conjugated sets of faults, and consistent with an about N–S direction of shortening (red large arrows in Fig. 9A). These faults offset vertical strata belonging to the southern limb of a major ENE-WSW-trending anticline. Faults with similar attitude and kinematics have been found elsewhere along this fold, suggesting they may represent a post-folding prosecution of shortening occurring mainly by brittle tectonics.

Nearby, at the site of Fig. 9B, several reverse faults have been observed in vertical outcrops. They are composed of two sets: one dipping about 30° northwards, and another set with similar geometry. Both sets affect the same southern limb of the anticline with offsets ranging from a few centimeters to some decimeters. They show mutual cross-cutting relationships and thus, as conjugated sets, are consistent with an about N–S direction of shortening (red large arrows in Fig. 9B). Similar

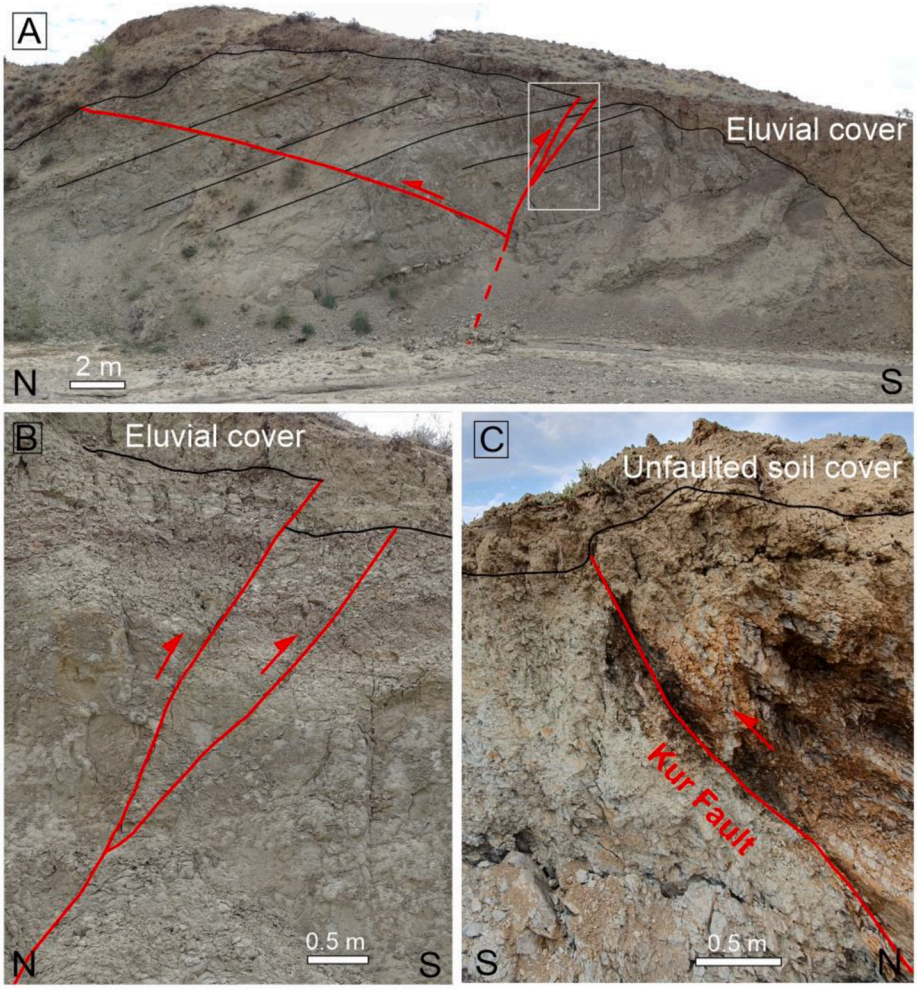

Fig. 8. (A) Sequence of tilted deposits of Early Pleistocene age showing a wedge structure delimited by two converging reverse faults. This outcrop is located near the trace of the Kur Fault. Note that the main fault dipping to the north offsets also the base of Holocene deposits, as can be seen in the detail of Figure (B). (C) Exposure of the plane of the Kur Fault in a trench. The recentmost eluvial/soil cover seems to be affected by fractures in correspondence of the upper projection of the Kur Fault plane, but a clear offset cannot be seen. Location in Fig. 3.

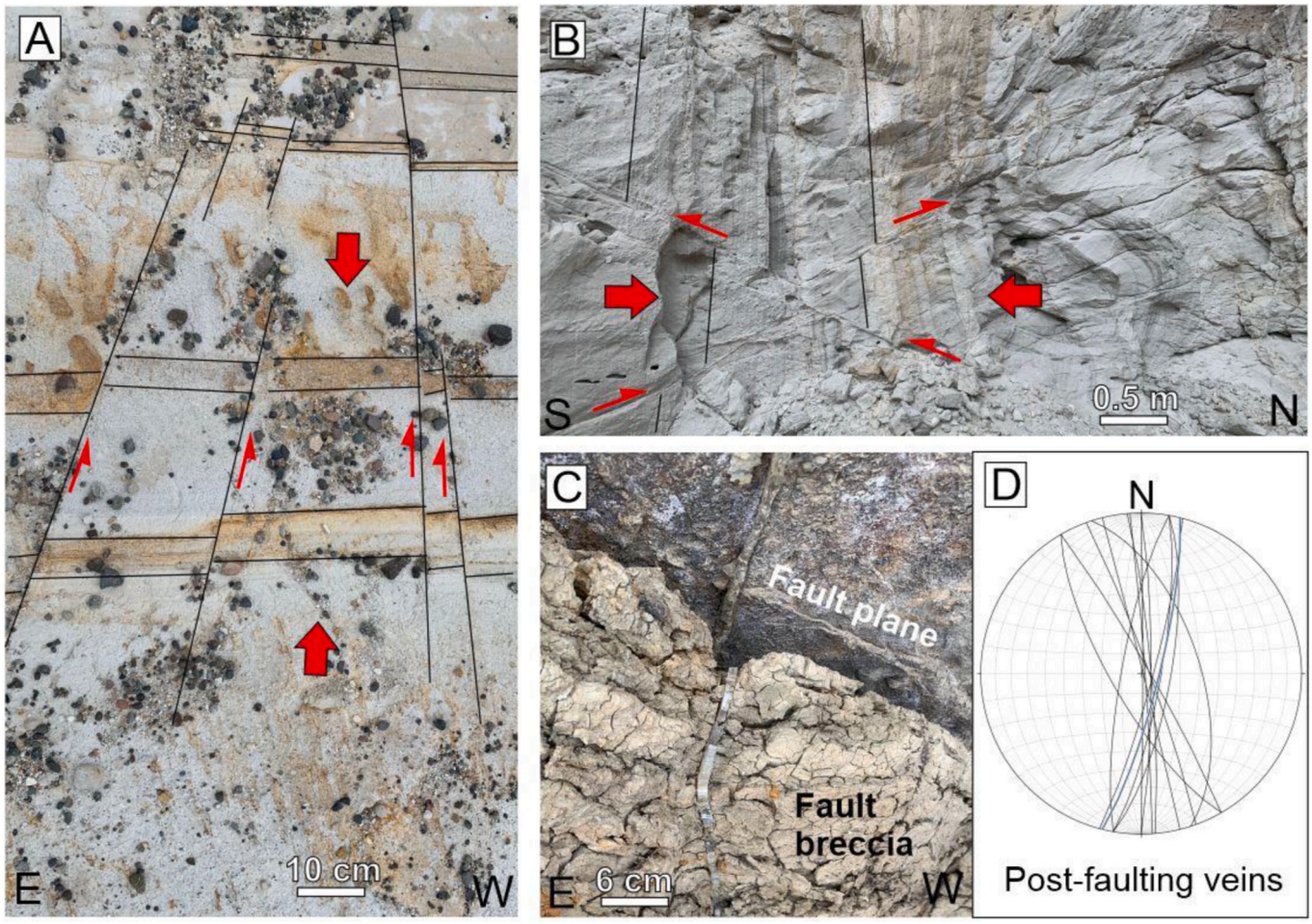

Fig. 9. (A) Strike-slip microfaults observed on a horizontal outcrop; note that NNW-SSE right-lateral strike-slip faults and NNE-SSW left-lateral strike-slip faults are consistent with an about N–S direction of shortening (large red arrows). (B) Reverse faults observed on a vertical outcrop, compatible with an about N–S direction of shortening (large red arrows). (C) Vein cutting across an E-W reverse fault. The 1-cm-offset of the vein is due to gravitational movement induced by artificial excavation. (D) Stereographic plot on the lower Schmidt emisphere of planes of post-faulting veins. Location in Fig. 3. (For interpretation of the references to colour in this figure legend, the reader is referred to the Web version of this article.)

observations as those carried out at the strike-slip faults, suggest that these reverse faults postdate the fold development.

At the site of Fig. 9C, we found several veins with crystalline growth fibres. In the same area there is a major fault dipping N170° with an inclination of 82°, characterized by a fault gouge of severel dm of thickness. This fault has tectoglyphes indicating reverse motions, although its inclination suggests possible tilting of the plane. Some of the veins are offset by the fault, whereas other veins cut across the fault plane and affect the fault gouge. One of these veins affecting the fault gouge is shown in Fig. 9C; the 1-cm-offset of the vein along the fault plane is due to gravitational movement induced by artificial excavation of the outcrop. We report in Fig. 9D only the veins that postdate faulting; these veins strike between NNW-SSE and NNE-SSW and are from vertical to subvertical. The orientation of crystal fibers indicates about E-W extension.

4.2.4. *A seismic section of the Kur fault*

Due to its relevance for our study, in Fig. 10 we report an interpreted

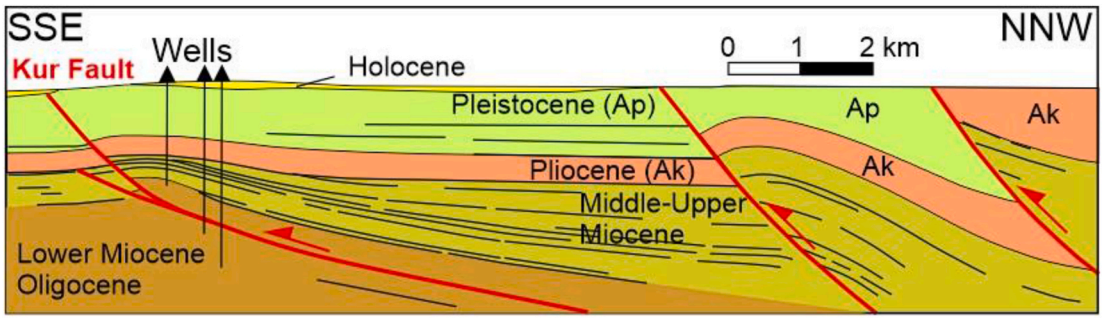

Fig. 10. Interpreted line drawing of seismic profile 86R110 across the eastern part of the Kur Fault (location of profile trace in Fig. 2). Ak, Akchagilian deposits (Pliocene); Ap, Apsheronian deposits (Pleistocene). Redrawn after Alania et al. (2017).

seismic profile of the eastern part of the studied fold-and-thrust belt from Alania et al. (2017). The profile incorporates results from three oil wells, located near the trace of the Kur Fault, which allowed to precisely date the deposits. The lower strata were attributed by Alania et al. (2017) to the Middle and Upper Miocene and show an increase in their thickness towards the north. These deposits create an anticline whose southern limb is offset by a fault with reverse motions. Above, the succession is composed of Pliocene strata that also show an anticline to the south and an asymmetric geometry with northward thickening. The closure of the fold limbs is higher in the lower strata. The southern limb of the Pliocene fold is also offset by the same fault that cuts also across the uppermost succession made of Pleistocene deposits. The same structure is repeated two times further the north, with the older deposits that become shallower and shallower.

It is worth underscoring that the southernmost fault depicted in the seismic profile reaches the surface in correspondence of the eastward surface trace of the Kur Fault. In this section, thus, the Kur Fault corresponds to a fault-propagation fold where the main fault plane splays upward with the shallower fault on the back. In the seismic section the shallower fault splay is interrupted by the Holocene deposits, but it is worth reminding that seismic data become less precise at shallower depths.

4.3. Earthquake distribution

The epicenters of instrumental earthquakes for the Kura fold-and-thrust belt and sourrounding area are shown in Fig. 11 with magnitudes and depths. Here it can be appreciated the widespread distribution of seismicity in the whole region, as well as the presence of low to moderate seismic activity also in the studied part of the Kura fold-and-thrust belt. Seismicity of greater magnitude is present outside the studied area with maximum Mw of 7.0 Some clusters of epicenters are present, especially elongated in a NW-SE direction, coherent with the general trend of the Quaternary faults. Their kinematics suggests that the clusters of seismic events in the southwestern part of the region is linked with transcurrent tectonics, whereas reverse kinematics dominates in all the remaining areas.

The frequency of seismicity increases wth depth, with the highest presence of earthquakes in the seismic layer of 10.1–20 km (Fig. 11C). The shallowest earthquakes dominate in the western part of the studied sector of the Kura fold-and-thurst belt (Fig. 11A), whereas in the eastern part deeper seismic events dominate (Fig. 11B and C). A cluster of seismic events is present NE of the studied belt and can be considered linked to other structures belonging to the frontal part of the Greater Caucasus.

The historical earthquake epicenter data in the same regional area are shown in Fig. 12, where it is possible to observe the presence of historical seismic activity around the study area and its absence inside this area. Historical earthquakes in the sourrounding area reached a maximum Ms of 7.4.

4.4. Earthquake focal mechanism solutions and state of stress

A map containing the new calculated FMS of the studied sector of the Kura fold-and-thrust belt is shown in Fig. 12. They show the presence of earthquakes with a pure reverse to slightly traspressional kinematics (7 events), followed by more pronounced traspressional kinematics (6 events). The directions of P axes are mostly from N–S to NE-SW. The depth of these events is comprised between 4 and 25 km.

The same Fig. 12 reports also the directions of horizontal compression, desumed by other published FMS (Tsereteli et al., 2016, 2021; Tibaldi et al., 2020) and by the World Stress Map (www.world-stress-map.org/) of the surrounding area including eastern Greater and Lesser Caucasus, in order to have a regional perception of the ongoing state of stress. Main Quaternary faults, classified by their kinematics, indicate mostly strike-slip type, and minor reverse faults, in the Lesser Caucasus, especially in the Armenian territory. In the Greater Caucasus and in the intermonate valley, there are mostly reverse faults. The directions of the greatest principal stress (σ_1) show some scattering although in the Greater Caucasus and in the intermontane valley they tend to concentrate in the range N–S to NE-SW, with a maximum oriented NNE-SSW at all crustal depths, as can be seen in the rose diagrams of Fig. 12.

4.5. Evidence of the Kur fault from ambient vibrations measurements

For the measurements across the fault scarp, five examples H/V spectral curves (15 in total) are plotted along the measurement profile in Fig. 13. Resonance peaks across the fault scarp can be well identified, indicating that a clearly softer deposit overlays a harder one; most likely this superficial soft material is made of fluvial deposits. Further, all sites are marked by lowest resonance frequencies larger than 2.5 Hz. This means that for an assumed shear-wave velocity (Vs) of the fluvial deposits and underlying soft or weathered sediments (typically marked by $200 < Vs < 400$ m/s), the combined near surface layers present on those sites are in total less than 35 m thick (using Equation (1) to compute the thickness 'h' – see also examples of thickness calculations in Fig. 13).

Both frequency peaks disappear for two measurements in the central part of the fault scarp, indicating that no contrast can be found under those measurement points (7 and 8, example shown for H/V curve 8 in Fig. 13). Outside the 50–70 m broad fault zone (distance between points AZ_AF_7 and _8). The higher frequency peak at 6–10 Hz indicates the presence of young allvuvial deposits (comparing those data with field observations near the section along the river in the east) with a thickness of less than 12 m, making up the upper part of the total soft sediment layer (using a value for Vs of 240 m/s for the calculation of 'h1'). The existence of this second resonance frequency indicates a contrast with the underlying weathered sediments (with $300 < Vs < 400$ m/s). Both soft sediment layers together are likely to produce the fundamental frequency peak on all sites outside the scarp area between 3 and 5 Hz, which corresponds to a total thickness of the near surface layers of 15–25 m (using an average Vs of 300 m/s for those two layers). The light coloured logs represent the thickness, h1, calculated from the higher frequency peak, f1, and the combined light and darker brown coloured logs show the total near surface layer thickness, h0, calculated from the lower frequency peak, f0, along the profile in Fig. 13. The lack of contrast between measurements points 7 and 8, together with the reconstructed shallow stratigraphy along the remaining section, suggest that the fault movements mixed up the layers and thus destroyed the layer interfaces and the Vs contrast, and/or that the rocks of the hangingwall block uplifted along the reverse fault and surmounted the river deposits located in the footwall block (i.e. to the south of the fault zone).

5. Discussion

5.1. Surface expression of the Kur fault

Rarely named in the literature (e.g. Onur et al., 2020), in the 1:500,000 Geological Map of Azerbaijan of Ali-Zadeh et al. (1975), the Kur Fault is represented with a continous line corresponding to a length of about 100 km. Partial traces of the fault, instead, have been reported in the 1:500,000 Geological Map of Caucasus of Nalivkin (1976a) in the form of two fault segments, one 26-km-long and the other one 20-km-long. In the Geological Map of Azerbaijan, at a scale of 1:500,000 of Bairamov (2008), the Kur Fault is reported with a discontinues line that shows three fault segments in left-stepping arrangement, for a total length of about 85 km. In the most recently published map, the Geological Map of Caucasus at 1:1,000,000 scale (Adamia et al., 2010), there is no trace of this fault, although some parallel and shorter faults are reported further north in the interior of the Kura fold-and-thust belt. In the 1:1,000,000 geological-structural map of the Kura fold-and-thrust belt of Forte et al. (2010), only two fault segments are reported, each one

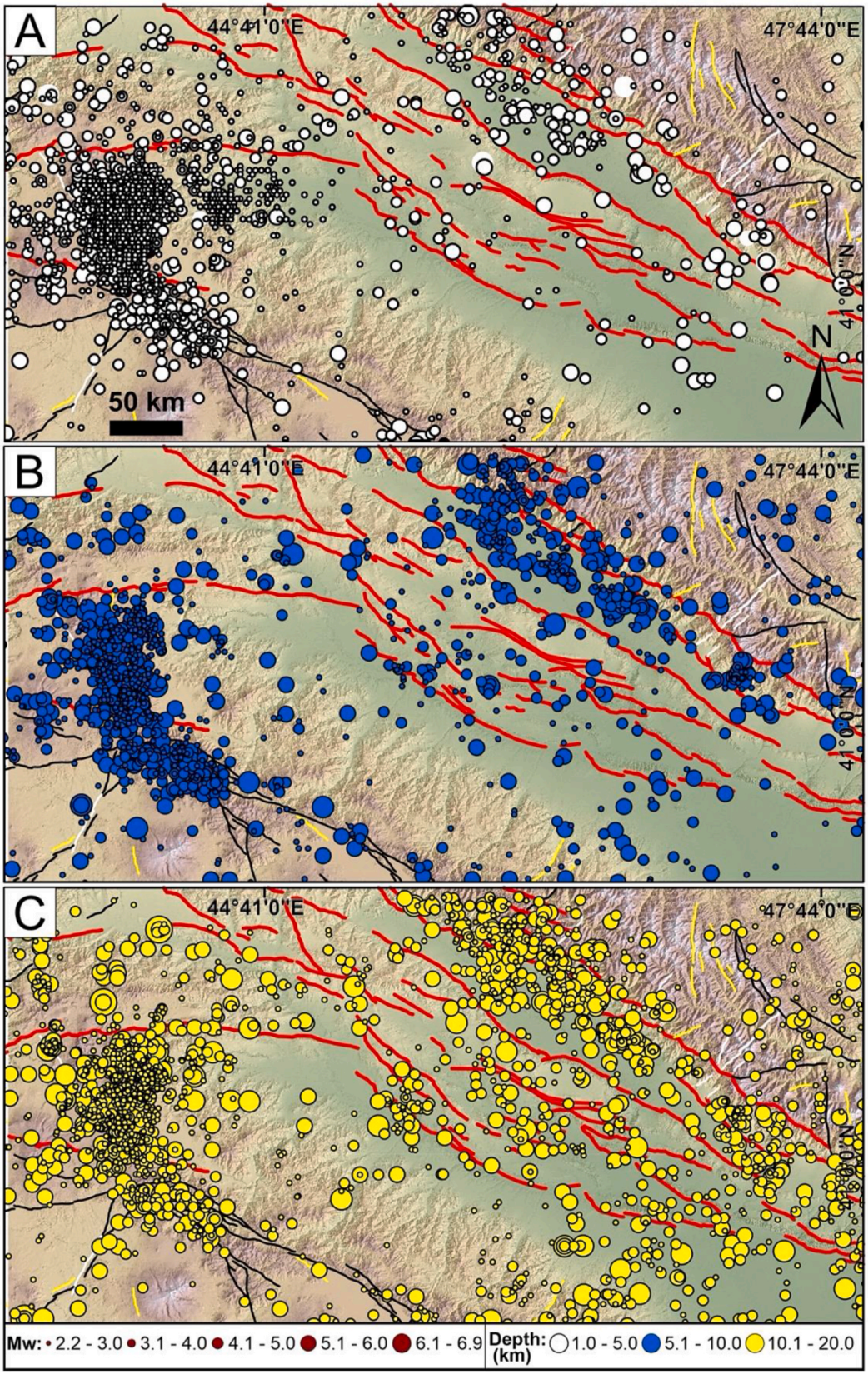

Fig. 11. Map of distribution of instrumental earthquakes with Magnitude and related depth: (A) 1–5 km, (B) 5.1–10 km, (C) 10.1–20 km. All data derive from a new catalogue assembled for this study. Faults are from our work for the studied area, and from the database of active faults of Eurasia of Zelenin et al. (2022) for all the surrounding region; red lines = reverse faults, black lines = strike-slip faults, white lines = normal faults, yellow lines = unclassified faults. (For interpretation of the references to colour in this figure legend, the reader is referred to the Web version of this article.)

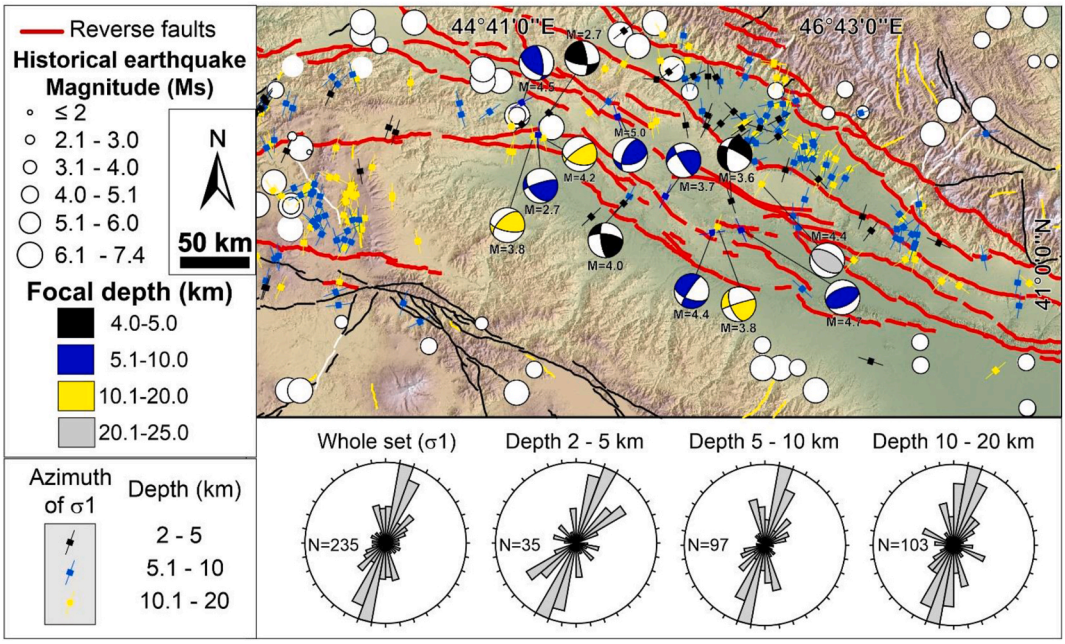

Fig. 12. Regional map of historical earthquakes epicentres (white circles), newly calculated earthquake focal mechanism solutions for the study area of the Kura fold-and-thrust belt divided by depth (coloured beach balls), and direction of σ_1 desumed from our catalogue of focal mechanisms and from data of the World Stress Map divided by depth. Rose diagrams show azimuthal distribution of σ_1. Faults are from our work for the studied area, and from the database of active faults of Eurasia of Zelenin et al. (2022) for all the surrounding region; red lines = reverse faults, black lines = strike-slip faults, white lines = normal faults, yellow lines = unclassified faults. (For interpretation of the references to colour in this figure legend, the reader is referred to the Web version of this article.)

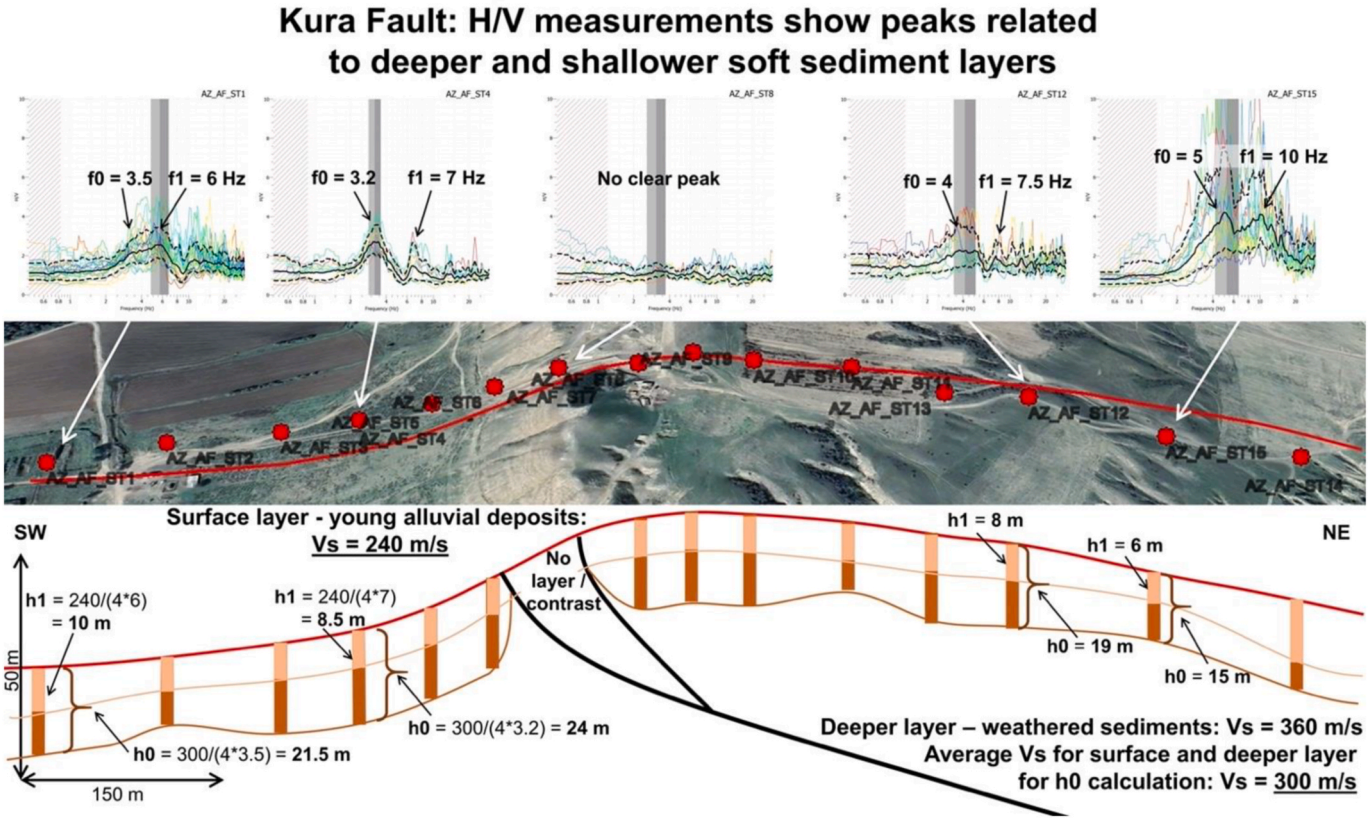

Fig. 13. Top and middle part of figure: Examples of five (out of 15) H/V measurements plotted along the measurement profile across the Kur Fault scarp. Lower part of figure: Distribution of the thickness logs calculated from the first and second peaks identified on the 15 H/V graphs; the light coloured logs corresponding to the shallow layer made of alluvial deposits with estimated Vs = 240 m/s, indicating the thickness h1 calculated from f1; the dark coloured logs represent the underling soft/weathered sediments with estimated Vs = 360 m/s. The total thickness of the light and dark coloured logs (see brackets, marking the total soft layer with average Vs of about 300 m/s) represents h0, calculated from f0.

about 25 km long, along the studied structure. Finally, in the database of active faults of Eurasia of Zelenin et al. (2022), a 131-km-long structure is reported along the trace of the Kur Fault but with a transcurrent kinematics. The georeferentation and superimposition of these maps in a GIS showed that the various traces of the fault are mostly not coincident, and the geometry of its surface trace remains uncertain.

In the present work, we mapped with the best possible detail, considering the extension of the structure, the possible trace and surface expression of the fault. A quite continuous scarp is present along the southern front of the Kura fold-and-thrust belt, being this scarp the expression of different arrangements of the Kur Fault near the surface. Hereunder we provide a brief summary of its main characteristics from west to east.

Along the border with Georgia (westernmost part of Fig. 3A), the Kur Fault scarp starts in an area where folding seems to dominate, although the oucrops are extremely scarce. The scarp here can be interpreted as the expression of the southern fold limb, as sketched in Fig. 14A. This architecture can be followed for 17 km, and beyond that the strata show a monoclinal geometry with a dip towards NE. The strata here are clearly truncated and the escarpment can be referred to a real fault scarp together with the eroded succession of the hanging wall block (Fig. 14C). This last part is about 7 km long until the tip of the first fault segment (total length first fault segment 24 km). Here there is the first right step, after which the strata seem to be truncated again and dip NE, although outcrops are scarce. The fault scarp here is 8.2 km long, as far as the site of Fig. 4A (location in Fig. 3A), from which a clear fold crops out for a length of 5.8 km, until the tip of the second fault segment (total length of second segment 14 km). After another right step, the third fault segment starts with folded strata with the southern limb mostly truncated, following a geometry as portayed in Fig. 14B. Alternance of folds and truncated NE-dipping strata suggests that this fold with offset frontal limb characterizes an 11.5-km-long segment of the Kur Fault. From the area near the site of Fig. 8A, strata dip to the NE and are truncated along the scarp, suggesting that this is a 19.7 km long fault scarp (as in Fig. 14C). This is consistent with our finding of the fault plane at the site of Fig. 8C and with the results of the ambient vibrations measurements. At the site of Fig. 6A, this third fault segment (total length 31.3 km) terminates and after another right step it is replaced by the fourth and last segment. This fourth segment starts as a fault scarp, 7 km long, which interrupts the sequence of deposits that dip NE. This is consistent with the termination of the previous segment that was also classified as a fault scarp. Then an about 2-km-long fold crops out, followed by a section of difficult interpretation due to bad outcrops and logistical problems. Beyond that, the Shamkir Lake hides the fault trace. However, its prolongation further east can be hypothesized based on the presence of a series of aligned morphostructural highs that emerge out of the water in the northern part of the lake. Another aligned morphostructural high is present onshore near the dam of the Shamkir lake (site of Fig. 7A), where there is a clear fold. The structure is again hidden by the Yenikend Su Anbari artificial lake, whereas further east there is the seismic section of Fig. 10 that shows the presence again of the Kur Fault near the surface in the form of a fold with the offset frontal limb. The total length of this fourth segment is 54 km.

In conclusion, the surface architecture of the Kur Fault appears as an alternation of folds and fault scarps. The intersection between the fault and the topographic surface dominates in the central part of the Kur Fault. Towards the eastern and western parts, folding of the shallow succession dominates; these folds can be interpreted as fault-propagation folds or fault-offset folds. This means that we cannot exclude that at several parts of the Kur Fault, the fault plane is anyway very shallow, although the Kur structure is expressed in outcrop by folds. It cannot even be ruled out that the Kur Fault is a unique major slip plane that propagated upward, towards the front of the Kura fold-and-thrust belt, at different depths, along a total length of about 123 km of development. These different architectures of the Kur Fault are reflected also by the local topography, as evidenced by the topographic profiles measured at different sites along the fault strike (Fig. 15). In correspondence of the emersion of the fold, the topography is curved (profiles 1 and 8). At a fault-offset fold, the topography is more complex and interrupted by the scarp (profile 2), and at the sites of the fault emersion, its scarp is clearly visible (profiles 3–7).

It is worth mentioning that the uplift is greater in the hanging wall block above the central part of the Kur Fault, where the fault slip plane mainly reaches the surface. This can be noticed in the topographic profiles of Fig. 16 where the northwestern and southeastern parts of the frontal Kura fold-and-thrust belt have lower elevations than in the central part, with respect to the location of the fault plane. Together

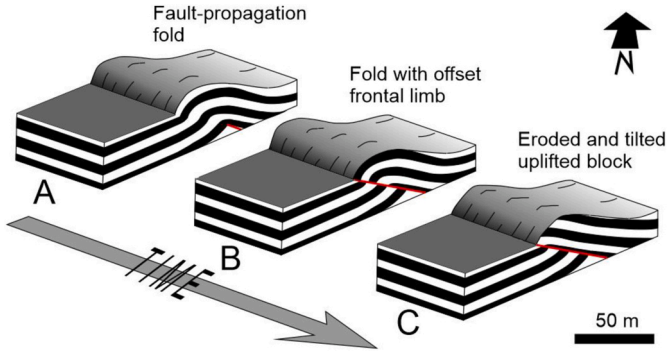

Fig. 14. Sketch of the three main surface expression of the Kur Fault. In (A) the scarp represents the southern limb of a fault-propagation fold. In (B) the scarp corresponds to the southern limb of the fold that is offset by the fault. In (C) the scarp represents the intersection between the fault and the topography together with the tilted succession in the hanging wall block that dips like the fault.

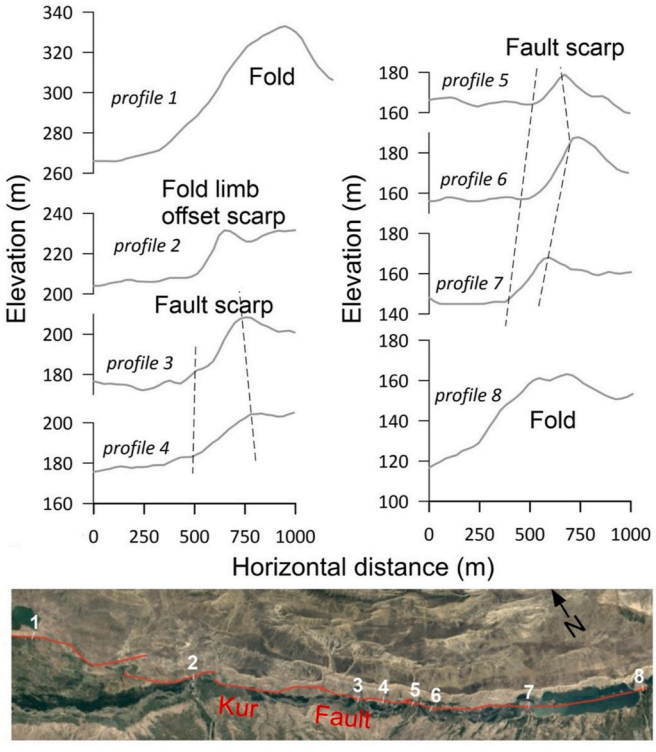

Fig. 15. Topographic profiles measured from the DEM at different sites along the Kur Fault. The inset shows the location of the various profiles and the trace (in red) of the Kur Fault. These profiles reflect the different architectures of the Kur Fault at the surface. Further explanations in the text. (For interpretation of the references to colour in this figure legend, the reader is referred to the Web version of this article.)

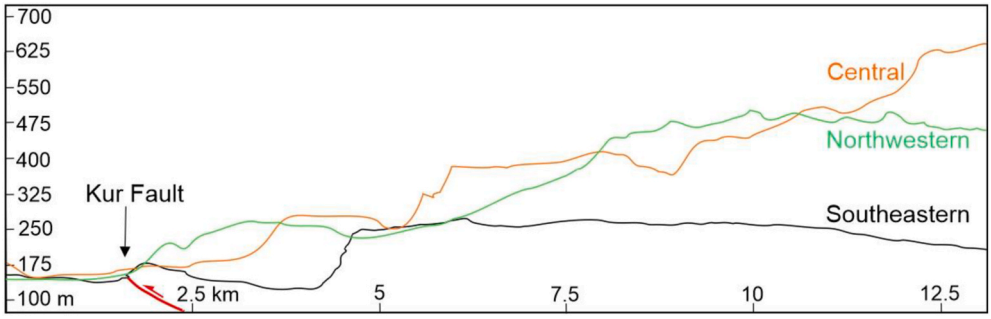

Fig. 16. Topographic profiles of the northwestern, central and southeastern part of the studied Kura fold-and-thrust belt. The southeastern profile (black) corresponds to the correct absolute altitudes a.s.l., whereas the other two profiles have been shifted to put the Kur Fault at the same altitude. This allows to have a direct comparison of the amount of uplift of the different parts of the belt.

with the presence at the surface of the Kur slip plane in the central part, this suggests that a larger slip cumulated along the central part of the fault. This can also be interpreted simply as along-strike variations in slip amount, or by the possibility that the northwestern and southeastern parts of the fault are still propagating.

5.2. Age of the Kur fault

Koçyiğit et al. (2001), based on field observations, indicate regional thrust-to-reverse fault controlled sedimentation since the Oligocene in the Transcaucasus basins. Again from a regional perspective, Ershov et al. (2003) indicate that during Late Miocene–Quaternary times, the eastern Transcaucasus basin underwent foreland-type asymmetrical subsidence linked to the loading of the Greater Caucasus that was rapidly uplifting. Forte et al. (2010) focusing on the Kura basin, concluded that compressional deformations here started in Pliocene times. Finally, Alania et al. (2017) based on the interpretation of several seismic sections and logs in the Georgian part of the Kura fold-and-thrust belt concluded that the compressional structures started to develop here in the Middle Miocene. With respect to these interpretations, we focus on the Kur Fault noting that the seismic section and wells portrayed in Fig. 10, show an increase in thickness towards the north of the Middle-Upper Miocene deposits; these growth strata indicate that in correspondence of this section of the Kur Fault, the compressional structures started to develop in the Middle Miocene. Similarly, also the Pliocene strata show an asymmetric geometry with northward thickening that confirms the prosecution of deformation here during this period. This is consistent with the gradual increase with depth of the interlimb angle of the associated fold. All this succession and the Pleistocene deposits are also faulted by the Kur plane, indicating a prosecution of deformation in Quaternary times. Of course we are aware that there are no available similar seismic sections for the remaining portion of the Kur Fault whose age of inception remains uncertain elsewhere.

Regarding our field observations, along the Kur Fault all the outcropping strata are involved in folding or are faulted. Folding definitively involves Upper Pliocene strata as well as Pleistocene deposits. In particular, the deformed deposits very rich in conglomerates interbedded with dark grey and reddish brown claystones corresponds to the section of the stratigraphic succession dated to the uppermost part of the Middle Pleistocene by Lazarev et al. (2019). We cannot exclude that conglomerates interlayered with lenses of sandstones might belong to the Upper Pleistocene as indicated by Alizadeh et al. (2016). In this case, the age of the fault activity, or the folding linked to the deeper fault, can be ascribed to the Holocene. We also found very loose conglomerate deposits that rest in discordance above Upper Pliocene and Pleistocene deposits; these conglomerates should thus have an age of latest Pleistocene-Holocene. This is confirmed by absolute datings of von Suchodoletz et al. (2016) who assign an age of 11.2 ka BP to the uppermost terraces of the Kura River immediately west of the Kur Fault. The uppermost conglomerate deposits are folded or faulted, thus suggesting recent deformation of Holocene age. Similarly, there are several fluvial terraces that are tilted up to 9° towards NNE and are uplifted along the Kur Fault. These terraces are composed of very loose conglomerates that must be also ascribed to the recentmost activity of the Kura River. We are thus inclined to consider the deformation of these terraces of Holocene age, as their tilting direction is consistent with uplift along a NNE-dipping reverse fault. Finally, in the site of Fig. 8B, we have found a secondary reverse fault with a geometry parallel to the main Kur Fault, located a few tens of meters north of the Kur Fault scarp, which offsets the recent colluvial cover.

All these data point to a quite long history of compressional deformations along the trace of the Kur Fault, with the youngest deformations that are in the form of surface folding and faulting of Holocene age. Considering the age of 11.2 ka BP (von Suchodoletz et al., 2016) for the youngest river terraces and the altitude of uplifted conglomerate deposits along the fault, we obtained an uplift rate of 1.6 mm/y to 3.75 mm/y for the Holocene.

5.3. Seismotectonics of the region and seismic hazard of the Kur fault

The Kura fold-and-thrust belt has been subject to compressional deformation that uplifted the Neogene-Quaternary succession up to hundreds of meters of altitude. The rock succession is now organized into a series of WNW- to NW-trending folds and reverse faults. Fault planes dominantly dip to the NNE, although very few backthrusts have been found in the field. Based on the orientation of the fold hinge lines and on the attitude of the various reverse faults, which locally show pure reverse motions, the general direction of shortening in the studied area ranges from N–S to NE-SW. The microtectonic field data indicate that after the formation of inclined to overturned anticlines, the strata of the vertical to overturned limbs are offset by pervasive strike-slip and reverse faults with small offsets. These secondary faults are consistent with an about N–S direction of shortening. A similar orientation of the horizontal greatest principal stress (σ_{Hmax}) can be desumed by the geometry of post-faulting veins collected in the field. Finally, the tectoglyphs measured on the Kur Fault indicate a N30° direction of shortening. Summarizing the above, the youngest directions of compression in the studied area are comprised between N0° and N30°.

In the studied part of the Kura fold-and-thrust belt, the new calculated crustal FMS indicate directions of shortening mostly between N–S and NE-SW (Fig. 12). This range is consistent with our field measurements and thus the FMS show a prolongation of the same state of stress from the Quaternary to the Present. The kinematics indicate the presence of reverse and transpressional faulting. The same range of active compression directions can be observed at a more regional scale, confirming the regional nature of the stress field. These data are consistent also with the analysis of the distribution of the P-axes for the seismic

events occurred in 2003–2017 in northern Azerbaijan, comprising the studied Kura fold-and-thrust belt, which indicates a dominant NE-SW direction of compression (Babayev et al., 2020). Tibaldi et al. (2020) developed a formal stress inversion of new and published FMS at the level of the whole Caucasus; in the central Kura basin, they calculated a N12° average direction of the present-day σ_1 that is horizontal. Tsereteli et al. (2016) also carried out a stress inversion of another set of FMS at the level of the Georgian part of the Caucasus. In correspondence of the here studied Kura fold-and-thrust belt, they calculated a N39° average direction of the σ_1.

The various data described in the previous sections indicate that at least part of the Kur Fault reached the surface, and thus it can be classified as a "capable fault", following the international nomenclature applied to active faults and especially Bryant and Hart (2007) who define as capable the faults that have ruptured the surface in the past 11 ka. From a seismotectonic point of view, the Kur Fault has strike and dip consistent with the general architecture of the Kura fold-and-thrust belt that developed by NNE-SSW to NE-SW crustal shortening. Above all, the Kur Fault plane and its detected motions (reverse with a pitch of 90°), are compatible with the present stress state both focusing on the Kura fold-and-thrust belt, as well as at more regional level. This means that this capable fault is also oriented compatibly with the stress state to be reactivated. We thus conclude that the Kur Fault is a structure that should be considered as potentially seismogenetic and has to be kept into consideration for its potential seismic hazard, especially considering its notable length. The presence of active motions is suggested also by the earthquake activity in the zone north of the surface trace of the Kur Fault (Fig. 11A–C). Here, statistical analyses of the seismicity should be carried out in order to assess the possible presence of hypocenter clouds that could "illuminate" the active fault plane, but this is out of the scope of the present work. It is noteworthy that historical large seismic events are missing exactly in the area north of the Kur Fault trace (Fig. 11A), suggesting that this fault might have long periods of quiescence. Although in theory the lacking of historical earthquakes here might be due to the fact that the Kura fold-and-thrust belt has been always poorly inhabited, we remind that large earthquakes should have been felt in the surrounding inhabited area.

Regarding the past surface rupture length of this fault, its trace is divided into four segments. We thus developed a calculation of the potential Magnitude (Mw) that can be released by a seismic event occurring along the whole length of 123 km of the structure, or by an earthquake produced by a single segment of the fault. Table 2 summarizes the main results of this calculation, which was based on Wells and Coppersmith (1994) and Blaser et al. (2010), for reverse faulting in continental crust. Our result of Mw 7.5 (based on Wells and Coppersmith, 1994) considering the possible whole length of rupture is consistent with Onur et al. (2020), although they did not explain the origin and type of their data on the Kur Fault.

Table 2
List of the Kur Fault segments (from West to East) and related calculated Mw both using Wells and Coppersmith (1994) and Blaser et al. (2010) formulae for reverse faulting in continental crust. The expected Mw for the entire Kur Fault is also given.

Wells and Coppersmith (1994)		Blaser et al. (2010)	
Fault scarp length (km)	Mw	Fault scarp length (km)	Mw
24.00	6.7	24.00	6.6
14.00	6.4	14.00	6.1
31.30	6.8	31.30	6.8
54.00	7.1	54.00	7.2
Kur Fault length (km)	**Mw**	**Kur Fault length (km)**	**Mw**
123	7.5	123	7.9

6. Conclusions

We studied the frontal structure, named Kur Fault, of the Plio-Quaternary Kura fold-and-thrust belt in the Greater Caucasus (Azerbaijan) by geological-structural and geomorphological surveys, integrated by a relocation of instrumental seismicity, data on historical seismicity, new focal mechanism solutions, and ambient vibrations measurements across the fault trace. The main results are.

- For the first time, the surface effects of this fault have been traced with precision in a GIS environment, resulting in a series of WNW-ESE-striking escarpments organized into four main segments, for a total length of 123 km. The segments show a right-stepping arrangement.
- The escarpments are the expression of different reorganization of shallow deposits in response to the upward propagation of the fault plane. Most parts of the central Kur scarp correspond to the presence of deposits tilted to the NNE associated to an emerging fault plane dipping in the same direction. This should represent the remaining part of eroded folds with the frontal (southern) limb offset by the fault, where maximum uplift occurred. Towards the external (northwestern and southeastern) parts of the Kur Fault, shallow folding dominates corresponding to fault-propagation folds.
- Analyses of the age of deformed deposits and landforms suggest activity as recent as the Holocene; a published seismic section (Alania et al., 2017) suggests inception in the Middle-Upper Miocene for the eastermont part of the faut.
- New and published focal mechanism solutions, and new microtectonic field observations indicate a Holocene and Present state of stress given by horizontal P-axes or σ_1 ranging N–S to N39°. The fault attitude and pure reverse kinematics, detected by field data, are coherent with this stress field, suggesting that the Kur Fault is in the seismotectonic conditions of potential reactivation.
- Calculation of potential Mw of the fault based on the length of the four fault segments indicates values in the range 6.7–7.1 based on Wells and Coppersmith (1994) rule, and 6.6–7.2 based on Blaser et al. (2010) rule, whereas for the whole Kur Fault Mw is 7.5 and 7.9 respectively.

In conclusion, the combination of surface observations with subsurface data indicates that the Kur Fault is given by the alignment of geologically active shallow folds and reverse slip planes, which represent the ongoing upward propagation of the deeper main fault plane. Present data do not allow to more precisely date the last seismic deformation along the fault, although our observations suggest a possible Holocene activity. Based on this, it is worth considering the potential of this fault for possible future reactivation and further paleoseismic investigations.

CRediT authorship contribution statement

Alessandro Tibaldi: Writing – original draft, Investigation, Funding acquisition. **Fabio Luca Bonali:** Writing – review & editing, Visualization, Project administration, Investigation. **Federico Pasquaré Mariotto:** Writing – review & editing, Investigation. **Paolo Oppizzi:** Investigation. **Nino Tsereteli:** Data curation. **Hans Havenith:** Writing – review & editing, Investigation. **Gulam Babayev:** Writing – review & editing. **Tomáš Pánek:** Writing – review & editing.

Declaration of competing interest

The authors declare that they have no known competing financial interests or personal relationships that could have appeared to influence the work reported in this paper.

Data availability

Data will be made available on request.

Acknowledgements

We acknowledge the useful suggestions of Editor Fabrizio Agosta, of Victor Alania and an anonymous reviewer on an earlier version of the manuscript. This study has been conducted in the framework of the 2022–2025 NATO project SPS G5907 “Prevention of Geo-Threats to Azerbaijan’s Energy Independence”.

References

Adamia, S., Chabukiani, A., Chkhotua, T., Sadradze, N., Zakaraia, S., Zakariadze, G., 2010. Geological Map of the Caucasus. Scale 1:1,000,000. University of Tbilisi, Georgia.

Adamia, S., Zakariadze, G., Chkhotua, T., Sadradze, N., Tsereteli, N., Chabukiani, A., Gventsadze, A., 2011. Geology of the caucasus: a review. Turk. J. Earth Sci. 20, 489–544.

Adamia, S., Alania, V., Tsereteli, N., Varazanashvili, O., Sadradze, N., Lursmanashvili, N., Gventsadse, A., 2017. Postcollisional tectonics and seismicity of Georgia. In: Sorkhabi, R. (Ed.), Tectonic Evolution, Collision, and Seismicity of Southwest Asia: in Honor of Manuel Barberian’s Forty-Five Years of Research Contributions, vol. 525. Geological Society of America Special Paper, pp. 535–572.

Agard, P., Omrani, J., Jolivet, L., Mouthereau, F., 2005. Convergence history across Zagros (Iran): constraints from collisional and earlier deformation. Int. J. Earth Sci. 94, 401–419.

Alania, V., Chabukiani, A., Chagelishvili, R., Enukidze, O., Gogrichiani, K., Razmadze, A., Tsereteli, N., 2017. Growth structures, piggy-back basins and growth strata of the Georgian part of the Kura foreland fold-thrust belt: implications for late Alpine kinematic evolution. In: Sosson, M., Stephenson, R.A., Adamia, S.A. (Eds.), Tectonic Evolution of the Eastern Black Sea and Caucasus, vol. 428. Geological Society, London, Special Publications, pp. 171–185.

Alania, V., Melikadze, G., Pace, P., Fórizs, I., Beridze, T., Enukidze, O., Giorgadze, A., Razmadze, A., 2022. Deformation structural style of the Rioni foreland fold-and-thrust belt, western Greater Caucasus: Insight from the balanced cross-section. Front. Earth Sci. 10, 10968386.

Ali-Zadeh, S.A., Bayramov, A.A., Gavrilov, D.M., Ibragimova, N.S., Mamedov, A.V., Shirinov ринов, F.Sh, 1975. The Map of Quaternary Deposits of Azerbaijan SSR. Scale 1:500,000. M. Aerogeologiya, Ministry of Geology of USSR (in Russian).

Alizadeh, A.A., Guliyev, I.S., Kadirov, F.A., Eppelbaum, L.V., 2016. Geosciences of Azerbaijan. Volume I: Geology. Regional Geology Reviews. Springer International Publishing, Switzerland, p. 214.

Allen, M.B., Armstrong, H.A., 2008. Arabia-Eurasia collision and the forcing of mid-Cenozoic global cooling. Palaeogeogr. Palaeoclimatol. Palaeoecol. 265, 52–58.

Allen, M., Jackson, J., Walker, R., 2004. Late Cenozoic reorganization of the Arabia-Eurasia collision and the comparison of short-term and long-term deformation rates. Tectonics 23 (16), TC2008. https://doi.org/10.1029/2003TC001530.

Armijo, R., Rauld, R., Thiele, R., Vargas, G., Campos, J., Lacassin, R., Kausel, E., 2010. The West andean thrust, the san ramón fault, and the seismic hazard for santiago, Chile. Tectonics 29, TC2007. https://doi.org/10.1029/2008TC002427.

Avagyan, A., Sosson, M., Karakhanian, A., Philip, H., Rebai, S., Rolland, Y., Melkonyan, R., Davtyan, V., 2010. Recent tectonic stress evolution in the Lesser Caucasus and adjacent regions. In: Sosson, M., Kaymakci, N., Stephenson, R.A., Bergerat, F., Starostenko, V. (Eds.), Sedimentary Basin Tectonics from the Black Sea and Caucasus to the Arabian Platform, vol. 340. Geological Society, London, Special Publications, pp. 393–408.

Babayev, G., Yetirmishli, G., Kazimova, S., Kadirov, F., Telesca, L., 2020. Stress field pattern in the Northeastern part of Azerbaijan. Pure Appl. Geophys. 177, 2739–2751.

Babayev, G.R., Agayeva, S.T., 2021. Strong earthquakes in Azerbaijan for historical and contemporary periods (conceptual review). Geofiz. Zh. Orig. 43 (3), 106–122.

Bairamov, A.A., 2008. Geological Map of Azerbaijan Republic, Scale 1:500,000. other 14 authors. National Academy of Science of Azerbaijan Republic.

Banks, C.J., Robinson, A.G., Williams, M.P., 1997. Structure and regional tectonics of the Achara-Trialet fold belt and the adjacent Rioni and Kartli foreland basins, Republic of Georgia. In: Robinson, A.G. (Ed.), Regional and Petroleum Geology of the Black Sea and Surrounding Region, vol. 68. American Association of Petroleum Geologists Memoir, pp. 331–346.

Bard, P.-Y., et al., 1999. Microtremor measurements : a tool for site effect estimation. The effects of surface geology on seismic motion 3, 1251–1279.

Berberian, M., 1997. Seismic sources of the Transcaucasian historical earthquakes. *Historical and prehistorical earthquakes in the Caucasus*. NATO ASI Series 28, 233–311.

Blaser, L., Krüger, F., Ohrnberger, M., Scherbaum, F., 2010. Scaling relations of earthquake source parameter estimates with special focus on subduction environment. Bull. Seismol. Soc. Am. 100 (6), 2914–2926.

Bonini, M., 2001. Passive roof thrusting and forelandward fold propagation in scaled brittle-ductile physical models of thrust wedges. J. Geophys. Res. 106 (B2), 2291–2311.

Bonnefoy-Claudet, S., 2004. Nature du bruit de fond sismique : implications pour les études des effets de site. Thèse de doctorat. Université Joseph-Fourier - Grenoble I, Grenoble, p. 241.

Bryant, W.A., Hart, E.W., 2007. Fault-Rupture hazard zones in California. Alquist-priolo earthquake fault zoning act with index to earthquake fault zones maps. California Geological Survey, spec. Publ. 42, 42.

Bull, W.B., McFadden, L., 1977. Tectonic geomorphology north and south of the garlock fault, California. In: O Dohering, D. (Ed.), Geomorphology in Arid Regions, Publ. Geomorphology, State University of New York, Binghamton, pp. 115–138.

Bull, W.B., 2007. Tectonic Geomorphology of Mountains. A New Approach to Paleoseismology. Blackwell Publishing, Oxford.

Burbank, D.W., Anderson, R.S., 2001. Tectonic Geomorphology. Blackwell Scientific Publications, Oxford.

Butler, R.W., 1982. The terminology of structures in thrust belts. J. Struct. Geol. 4 (3), 239–245.

Chapple, W.M., 1978. Mechanics of thin-skinned fold-and-thrust belts. Geol. Soc. Am. Bull. 89 (8), 1189–1198.

Coward, M.P., De Donatis, M., Mazzoli, S., Paltrinieri, W., Wezel, F.C., 1999. Frontal part of the northern Apennines fold and thrust belt in the Romagna-Marche area (Italy): shallow and deep structural styles. Tectonics 18 (3), 559–574.

Davis, D., Suppe, J., Dahlen, F.A., 1983. Mechanics of fold-and-thrust belts and accretionary wedges. J. Geophys. Res. Solid Earth 88 (B2), 1153–1172.

Dean, S.L., Morgan, J.K., Fournier, T., 2013. Geometries of frontal fold and thrust belts: insights from discrete element simulations. J. Struct. Geol. 53, 43–53.

DeCelles, P.G., Gehrels, G.E., Quade, J., Kapp, P.A., Ojha, T.P., Upreti, B.N., 1998. Neogene foreland basin deposits, erosional unroofing, and the kinematic history of the Himalayan fold-thrust belt, western Nepal. Geol. Soc. Am. Bull. 110, 2–21. https://doi.org/10.1130/0017606(1998)110\0002:NFBDEU[2.3.CO;2.

Demanet, D., Renardy, F., Vanneste, K., Jongmans, D., Camelbeeck, T., Meghraoui, M., 2001. The use of geophysical prospecting for imaging active faults in the Roer Graben, Belgium. Geophysics 66 (1), 78–89. https://doi.org/10.1190/1.1444925.

Dotduyev, S.I., 1986. Nappe structure of the greater caucasus range. Geotectonics 20 (5), 420–430.

Ershov, A.V., Brunet, M.F., Nikishin, A.M., Bolotov, S.N., Nazarevich, B.P., Korotaev, M. V., 2003. Northern Caucasus basin: thermal history and synthesis of subsidence models. Sediment. Geol. 156 (1–4), 95–118.

Forte, A.M., Cowgill, E., Bernardin, T., Kreylos, O., Hamann, B., 2010. Late cenozoic deformation of the Kura fold-thrust belt, southern greater caucasus. Geol. Soc. Am. Bull. 122, 465–486.

Forte, A.M., Cowgill, E., Murtuzayev, I., Kangarli, T., Stoica, M., 2013. Structural geometries and magnitude of shortening in the eastern Kura fold-thrust belt, Azerbaijan: implications for the development of the Greater Caucasus Mountains. Tectonics 32, 688–717.

Forte, A.M., Cowgill, E., Whipple, K.X., 2014. Transition from a singly vergent to doubly vergent wedge in a young orogen: the Greater Caucasus. Tectonics 33 (11), 2014TC003651.

Forte, A.M., Whipple, K.X., Cowgill, E., 2015. Drainage network reveals patterns and history of active deformation in the eastern Greater Caucasus. Geosphere 11, 1343–1364.

Hammerstein, J.A., Di Cuia, R., Cottam, M.A., Zamora, G., Butler, R.W., 2020. Fold and thrust belts: structural style, evolution and exploration–an introduction. Geological Society, London, Special Publications 490 (1), 1–8.

Havenith, H.B., Jongmans, D., Faccioli, E., Abdrakhmatov, K., Bard, P.Y., 2002. Site effect analysis around the seismically induced Ananevo rockslide, Kyrgyzstan. Bull. Seismol. Soc. Am. 92 (8), 3190–3209. https://doi.org/10.1785/0120010206.

Hung, J.H., Wiltschko, D.V., Lin, H.-C., Hickman, J., Fang, P., Bock, Y., 1999. Structure and motion of the southwestern taiwan fold and thrust belt. TAO 10 (3), 543–568.

Ismail-Zadeh, A., Adamia, S., Chabukiani, A., Chelidze, T., Cloetingh, S., Floyd, M., Gorshkov, A., Gvishiani, A., Ismail-Zadeh, T., Kaban, M.K., Kadirov, F., Karapetyan, J., Kangarli, T., Kiria, J., Koulakov, I., Mosar, J., Mumladze, T., Müller, B., Sadradze, N., Safarov, R., Schilling, F., Soloviev, A., 2020. Geodynamics, seismicity, and seismic hazards of the Caucasus. Earth Sci. Rev. 207, 103222 https://doi.org/10.1016/j.earscirev.2020.103222.

Jackson, J., 1992. Partitioning of strike-slip and convergent motion between Eurasia and Arabia in eastern Turkey. J. Geophys. Res. 97, 12471–12479.

Jones, P.B., 1996. Triangle zone geometry, terminology, and kinematics. Bull. Can. Petrol. Geol. 44 (2), 139–152.

Kadirov, F., Floyd, M., Alizadeh, A., Guliev, I., Reilinger, R., Kuleli, S., King, R., Nafi Toksoz, M., 2012. Kinematics of the eastern caucasus near baku, Azerbaijan. Nat. Hazards 63, 997–1006.

Kadirov, F., Floyd, M., Reilinger, R., Alizadeh, AkA., Guliyev, I.S., Mammadov, S.G., Safarov, R.G., 2015. Active geodynamics of the Caucasus region: implications for earthquake hazards in Azerbaijan. Proc. Azerb. Nat. Acad. Sci., Sci. Earth 3, 3–17.

Kadirov, F., Mammadov, S., Reilinger, R., McClusky, S., 2008. Some new data on modern tectonic deformation and active faulting in Azerbaijan (according to Global Positioning System measurements). Proc. Azerbaijan Natl. Acad. Sci. Earth’s Sci. 1, 82–88.

Kangarli, T.N., Kadirov, F.A., Etirmishli, G.D., Aliev, F.A., Kazimova, S.E., Aliev, A.M., Safarov, R.T., Vakhabov, U.G., 2018. Geodynamics, active faults and earthquake source mechanisms in the zone of pseudosubduction interaction of continental microplates in the South and North Caucasus (southern slope of the Greater Caucasus, Azerbaijan). Geodyn. Tectonophys. 9, 1099–1126. https://doi.org/10.5800/GT-2018-9-4-0385.

Karakhanian, A., Vernant, P., Doerflinger, E., Avagyan, A., Philip, H., Aslanyan, R., Champollion, C., Arakelyan, S., Collard, P., Baghdasaryan, H., Peyret, M.,

Davtyan, V., Calais, E., Masson, F., 2013. GPS constraints on continental deformation in the Armenian region and Lesser Caucasus. Tectonophysics 592, 39–45.
Keller, E.A., Pinter, N., 2002. Active Tectonics: Earthquakes, Uplift, and Landscape, second ed. Prentice Hall.
Koçyiğit, A., Yılmaz, A., Adamia, S., Kuloshvili, S., 2001. Neotectonics of east anatolia plateau (Turkey) and lesser caucasus: implication for transition from thrusting to strike-slip faulting. Geodin. Acta 14, 177–195.
Lachet, C., Bard, P.-Y., 1994. Numerical and theoretical investigations on the possibilities and limitations of Nakamura's Technique. J. Phys. Earth 42 (5), 377–397. https://doi.org/10.4294/jpe1952.42.377.
Lander, A.V., 2004. The FA2002 Program System to Determine the Focal Mechanisms of Earthquakes in Kamchatka, the Commander Islands and the Northern Kuriles. Report KEMSD GS RAS, Petropavlovsk-Kamchatsky, p. 250.
Lazarev, S., Jorissen, E., van de Velde, S., Rausch, L., Stoica, M., Wesselingh, F., Van Baak, C., Yanina, T., Aliyeva, E., Krijgsman, W., 2019. Magneto-biostratigraphic age constraints on the palaeoenvironmental evolution of the South Caspian basin during the Early-Middle Pleistocene (Kura basin, Azerbaijan). Quat. Sci. Rev. 222 https://doi.org/10.1016/j.quascirev.2019.105895.
Lee, W., Larh, S., 1975. HYPO-71 (Revised): a Computer Program for Determining Hypocenter, Magnitude and First-Motion Pattern of Local Earthquakes. U.S. Geological Survey Open File. Report 75-311.
McCalpin, J.P., Carver, G.A., 2009. Paleoseismology of compressional tectonic environments. Int. Geophys. 95, 315–419.
McQuarrie, N., van Hinsbergen, D.J.J., 2013. Retrodeforming the Arabia-Eurasia collision zone: age of collision versus magnitude of continental subduction. Geology 41, 315–318.
Mosar, J., Kangarli, T., Bochud, M., Glasmacher, U.A., Rast, A., Brunet, M.F., Sosson, M., 2010. Cenozoic–recent tectonics and uplift in the greater caucasus: a perspective from Azerbaijan. In: Sosson, M., Kaymakci, N., Stephenson, R.A., Bergerat, F., Starostenko, V. (Eds.), Sedimentary Basin Tectonics from the Black Sea and Caucasus to the Arabian Platform, vol. 340. Geological Society, London, Special Publication, pp. 261–280.
Mugnier, J.L., Huyghe, P., Gajurel, A.P., Becel, D., 2005. Frontal and piggy-back seismic ruptures in the external thrust belt of Western Nepal. J. Asian Earth Sci. 25 (5), 707–717.
Mukul, M., 2000. The geometry and kinematics of the Main Boundary Thrust and related neotectonics in the Darjiling Himalayan fold-and-thrust belt, West Bengal, India. J. Struct. Geol. 22 (9), 1261–1283.
Nakamura, Y., 1989. A method for dynamic characteristics estimation of subsurface using microtremor on the ground surface. Railway Technical Research Institute, Quarterly Reports 30 (1).
Nalivkin, D.V., 1976a. Geologic Map of the Caucasus (In Russian): Ministry of Geology, Union of Soviet Socialist Republics scale 1:500,000.
Nalivkin, V.D., 1976b. Dynamics of the development of the Russian platform structures. Dev. Geotectonics 12, 247–262.
Nikonov, A.A., 1982. A very powerful earthquake in the greater caucasus mountains, january 14, 1668. Izvestiya Phys. Solid Earth 18, 713–724.
Nogoshi, M., Igarashi, T., 1970. On the propagation characteristics of microtremors. J. Seism. Soc. Japan 23, 264–280.
Okay, A.I., Zattin, M., Cavazza, W., 2010. Apatite fission-track data for the Miocene Arabia-Eurasia collision. Geology 38, 35–38.
Onur, T., Gok, R., Godoladze, T., Gunia, I., Boichenko, G., Buzaladze, A., Tumanova, N., Dzmanashvili, M., Sukhishvili, L., Javakishvili, Z., Cowgill, E., Bondar, I., Yetirmishli, G., 2019. Probabilistic Seismic Hazard Assessment for Georgia (No. LLNL-TR-771451). Lawrence Livermore National Lab., Livermore, CA, USA.
Onur, T., Gok, R., Godoladze, T., Gunia, I., Boichenko, G., Buzaladze, A., Tumanova, N., Dzmanashvili, M., Sukhishvili, L., Javakishvili, Z., Cowgill, E., Bondár, I., Yetirmishli, G., 2020. Probabilistic seismic hazard assessment using legacy data in Georgia. Seismol Res. Lett. 91 (3), 1500–1517.
Pandey, M.R., Tandukar, R.P., Avouac, J.P., Lavé, J., Massot, J.P., 1995. Evidence for recent interseismic strain accumulation on a mid-crustal ramp in the central Himalaya of Nepal. Geophys. Res. Lett. 22, 751–758. https://doi.org/10.1029/94GL02971.
Pánek, T., Březný, M., Havenith, H.B., Tibaldi, A., 2024. Landslides and growing folds: a lesson from the Kura fold-and-thrust belt (Azerbaijan, Georgia). Geomorphology 449, 109059.
Pasquarè Mariotto, F., Tormey, D., Vezzoli, L., Okrostsvaridze, A., Tutberidze, B., 2011. Mitigating the consequences of extreme events on strategic facilities: evaluation ofvolcanic and seismic risk affecting the Caspian oil and gas pipelines in the Republic of Georgia. J. Environ. Manag. 92, 1774–1782.
Philip, H., Cisternas, A., Gvishiani, A., Gorshkov, A., 1989. The Caucasus: an actual example of the initial stages of continental collision. Tectonophysics 161, 1–21. https://doi.org/10.1016/0040-1951(89)90297-7.
Pierce, I., Guliyev, I., Yetirmishli, G.J., Muradov, R., Kazimova, S., Javanshir, R., Johnson, B., Marshall, N., Walker, R.T., Wordsworth, P., 2022. Surface rupturing earthquakes of the greater caucasus frontal thrusts, Azerbaijan. Author. https://doi.org/10.22541/essoar.167152213.30022523/v1 submitted for publication.
Rajendran, C.P., John, B., Rajendran, K., 2015. Medieval pulse of great earthquakes in the central Himalaya: viewing past activities on the frontal thrust. J. Geophys. Res. Solid Earth 120 (3), 1623–1641.
Rautian, T.G., 1964. On the determination of the energy of earthquakes at a distance of 3000 km. Eksperimental'naia seismika. Trudy IFZ ANSSSR (32), 199.
Rautian, T.G., Khalturin, V.I., 1978. The use of the coda for determination of the earthquake source spectrum. Bull. Seismol. Soc. Am. 68 (4), 923–948.
Reilinger, R., Barka, A., 1997. GPS constraints on fault slip rates in the Arabia-Africa-Eurasia plate collision zone: implications for earthquake recurrence times. In: Giardini, D., Balassanian, S. (Eds.), Historical and Prehistorical Earthquakes in the Caucasus. Kluwer Academic, Dordrecht, pp. 91–108.
Reilinger, R., McClusky, S., Vernant, P., Lawrence, S., Ergintav, S., Çakmak, R., Özener, H., Kadirov, F., Guliev, I., Stepanyan, R., Nadariya, M., Hahubia, G., Mahmoud, S., Sakr, K., Ar Rajehi, A., Paradissis, D., Al-Aydrus, A., Prilepin, M., Guseva, T., Evren, E., Dmitrotsa, A., Filikov, S.V., Gomez, F., Al-Ghazzi, R., Karam, G., 2006. GPS constraints on continental deformation in the Africa–Arabia–Eurasia continental collision zone and implications for the dynamics of plate interactions. J. Geophys. Res. 111, B05411. https://doi.org/10.1029/2005JB004051.
Saintot, A., Brunet, M.-F., Yakovlev, F., Sebrier, M., Stephenson, R.A., Ershov, A.V., Chalot-Prat, F., McCann, T., 2006. The mesozoic–cenozoic tectonic evolution of the greater caucasus. In: Gee, D.G., Stephenson, R.A. (Eds.), European Lithosphere Dynamics, vol. 32. Geological Society, London, Memoir, pp. 277–289.
Seeber, L., Armbruster, J., 1981. Great detachment earthquakes along the Himalayan Arc and long-term forecasting. In: Simpson, D.W., Richards, P.G. (Eds.), Earthquake Prediction: an International Review, Maurice Ewing Ser., vol. 4. AGU, pp. 259–277.
Smeraglia, L., Fabbri, O., Choulet, F., Buatier, M., Boulvais, P., Bernasconi, S.M., Castorina, F., 2020. Syntectonic fluid flow and deformation mechanisms within the frontal thrust of a foreland fold-and-thrust belt: example from the Internal Jura, Eastern France. Tectonophysics 778, 228178.
Sokhadze, G., Floyd, M., Godoladze, T., King, R., Cowgill, E.S., Javakhishvili, Z., Hahubia, G., Reilinger, R., 2018. Active convergence between the Lesser and Greater Caucasus in Georgia: constraints on the tectonic evolution of the Lesser-Greater Caucasus continental collision. Earth Planet Sci. Lett. 481, 154–161.
Sukhishvili, L., Forte, A.M., Merebashvili, G.L.J., Whipple, K.X., Javakhishvili, Z., Heimsath, A., Godoladze, T., 2021. Active deformation and Plio-Pleistocene fluvial reorganization of the western Kura fold–thrust belt, Georgia: implications for the evolution of the Greater Caucasus Mountains. Geol. Mag. 158, 583–597.
Suppe, J.O.H.N., Namson, J., 1979. Fault-bend origin of frontal folds of the western Taiwan fold-and-thrust belt. Petrol. Geol. Taiwan 16 (22), 1.
Takaku, J., Tadono, T., Doutsu, M., Ohgushi, F., Kai, H., 2020. Updates of 'AW3D30'ALOS global digital surface model with other open access datasets. Int. Arch. Photogram. Rem. Sens. Spatial Inf. Sci. 43, 183–189.
Tan, O., Taymaz, T., 2006. Active tectonics of the Caucasus: earthquake source mechanisms and rupture histories obtained from inversion of teleseismic body waveforms. In: Dilek, Y., Pavlides, S. (Eds.), Postcollisional Tectonics and Magmatism in the Mediterranean Region and Asia, vol. 409. Geological Society of America Special Paper, pp. 531–578.
Tari, G., Vakhania, D., Tatishvili, G., et al., 2018. Stratigraphy, structure and petroleum exploration play types of the Rioni Basin, Georgia. Geol. Soc. Lond. Spec. Publ. 464, 403–438.
Tavani, S., Storti, F., Lacombe, O., Corradetti, A., Muñoz, J.A., Mazzoli, S., 2015. A review of deformation pattern templates in foreland basin systems and fold-and-thrust belts: implications for the state of stress in the frontal regions of thrust wedges. Earth Sci. Rev. 141, 82–104.
Tevelev, A.V., Blyumkin, E.I., 1990. Comparative tectonics from space images of the Kura and Surkhandar'ya depressions. Sov. J. Rem. Sens. 7 (3), 509–516.
Thakur, V.C., Pandey, A.K., Suresh, N., 2007. Late quaternary-holocene frontal fault zone of the garhwal sub himalaya, NW India. J. Asian Earth Sci. 29, 305–319.
Tibaldi, A., Russo, E., Bonali, F.L., Alania, V., Chabukiani, A., Enukidze, O., Tsereteli, N., 2017a. 3-D anatomy of an active fault-propagation fold: a multidisciplinary case study from Tsaishi, western Caucasus (Georgia). Tectonophysics 717, 253–269.
Tibaldi, A., Alania, V., Bonali, F.L., Enukidze, O., Tsereteli, N., Kvavadze, N., Varazanashvili, O., 2017b. Active inversion tectonics, simple shear folding and back-thrusting at Rioni Basin, Georgia. J. Struct. Geol. 96, 35–53.
Tibaldi, A., Bonali, F.L., Russo, E., Pasquarè Mariotto, F., 2018. Structural development and stress evolution of an arcuate fold-and-thrust system, southwestern Greater Caucasus, Republic of Georgia. J. Asian Earth Sci. 156, 226–245.
Tibaldi, A., Tsereteli, N., Varazanashvili, O., Babayev, G., Barth, A., Mumladze, T., Bonali, F.L., Russo, E., Kadirov, F., Yetirmishli, G., Kazimova, S., 2020. Active stress field and fault kinematics of the Greater Caucasus. J. Asian Earth Sci. 188, 104108.
Tibaldi, A., Babayev, G., Bonali, F.L., Pasquaré Mariotto, F., Russo, E., Tsereteli, N., Corti, N., 2021. Active kinematics of the greater caucasus from seismological and GPS data: a review. Building Knowledge for Geohazard Assessment and Management in the Caucasus and other Orogenic Regions 33–57.
Tibaldi, A., de Nardis, R., Torrese, P., Bressan, S., Pedicini, M., Talone, D., Bonali, F.L., Corti, N., Russo, E., Lavecchia, G., 2023. A multi-scale approach to the recent activity of the Stradella thrust in the seismotectonic context of the Emilia Arc (northwestern Italy). Tectonophysics 857, 229853.
Trexler, C.C., Cowgill, E., Spencer, J.Q.G., Godoladze, T., 2020. Rate of active shortening across the southern thrust front of the Greater Caucasus in western Georgia from kinematic modeling of folded river terraces above a listric thrust. Earth Planet Sci. Lett. 544, 116362.
Trexler, C.C., Cowgill, E., Niemi, N.A., Vasey, D.A., Godoladze, T., 2022. Tectonostratigraphy and major structures of the Georgian Greater Caucasus: implications for structural architecture, along-strike continuity, and orogen evolution. Geosphere 18, 211–240.
Trexler, C., Cowgill, E., Vasey, D., Niemi, N., 2023. Total shortening estimates across the western Greater Caucasus mountains from balanced cross sections and area balancing. Tektonika 1 (2), 198–208.
Tsereteli, N., Danciu, L., Varazanashvili, O., Sesetyan, K., Qajaia, L., Sharia, T., Svanadze, D., Khvedelidze, I., 2021. The 2020 national seismic hazard model for Georgia (sakartvelo). In: Building Knowledge for Geohazard Assessment and Management in the Caucasus and Other Orogenic Regions. Springer, Netherlands, pp. 131–168.

Tsereteli, N., Tibaldi, A., Alania, V., Gventsadse, A., Enukidze, O., Varazanashvili, O., Muller, B.I.R., 2016. Active tectonics of central-western Caucasus, Georgia. Tectonophysics 691, 328–344.

Vann, I.R., Graham, R.H., Hayward, A.B., 1986. The structure of mountain fronts. J. Struct. Geol. 8 (3–4), 215–227.

Vasey, D.A., Cowgill, E., Roeske, S.M., Niemi, N.A., 2020. Evolution of the greater caucasus basement and formation of the main caucasus thrust. Tectonics 39, e2019TC005828. https://doi.org/10.1029/2019TC005828.

von Suchodoletz, H., Gärtner, A., Hoth, S., Umlauft, J., Sukhishvili, L., Faust, D., 2016. Late Pleistocene river migrations in response to thrust belt advance and sediment-flux steering—the Kura River (southern Caucasus). Geomorphology 266, 53–65.

Walker, R., Yetirmishli, G.J., Pierse, I., Kazimova, S.E., Kazimov, I.E., 2022. The first results of paleoseismological studies between oxford university and republican seismic survey center of Anas. Seismoprognosis Observations in the Territory of Azerbaijan 22 (2), 3–8.

Wathelet, M., 2005. GEOPSY geophysical signal database for noise array processing. Software, LGIT, Grenoble, France. https://www.geopsy.org/.

Wathelet, M., Chatelain, J.L., Cornou, C., Giulio, G.D., Guillier, B., Ohrnberger, M., Savvaidis, A., 2020. Geopsy : a user-friendly open-source tool set for ambient vibration processing. Seismol Res. Lett. 91 (3), 1878–1889. https://doi.org/10.1785/0220190360.

Wells, D.L., Coppersmith, K.J., 1994. New empirical relationships among magnitude, rupture length, rupture width, rupture area, and surface displacement. Bull. Seismol. Soc. Am. 84 (4), 974–1002.

Yetirmishli, G.J., Kazimov, I.E., Kazimova, A.F., 2022. Analysis of modern movements of Earth crust blocks in Azerbaijan according to the data of GPS stations in 2020-2021. Seism. Obs. Territ. Azerbaijan 21, 19–24.

Zelenin, E., Bachmanov, D., Garipova, S., Trifonov, V., Kozhurin, A., 2022. The Active Faults of Eurasia Database (AFEAD): the ontology and design behind the continental-scale dataset. Earth Syst. Sci. Data 14 (10), 4489–4503.